[redacted]

Copy 227

[redacted]

RM A52B06

53-28-49

NACA RM A52B06

TECH LIBRARY KAFB, NM

0142905

6375

NACA

RESEARCH MEMORANDUM

METHOD FOR ESTIMATING PITCHING-MOMENT INTERFERENCE OF WING-BODY COMBINATIONS AT SUPERSONIC SPEED

By George E. Kaattari, Jack N. Nielsen, and William C. Pitts

Ames Aeronautical Laboratory
Moffett Field, Calif.

Cancelled
NASA CN #1 (1-5)
[illegible]
GSH
GRADE OF
10 Jan 63
DATE

[redacted]

This material contai[redacted] Defense of the United States within the meaning of the espionage laws, [redacted] Secs. 793 and 794, the transmission or revelation of which in any manner to an unauthorized person is prohibited by law.

NATIONAL ADVISORY COMMITTEE FOR AERONAUTICS

WASHINGTON
April 17, 1952

319.98/13

[redacted]

PERMANENT

TECH LIBRARY KAFB, NM
0142905

 [redacted]

NATIONAL ADVISORY COMMITTEE FOR AERONAUTICS

RESEARCH MEMORANDUM

METHOD FOR ESTIMATING PITCHING-MOMENT INTERFERENCE OF WING-BODY COMBINATIONS AT SUPERSONIC SPEED

By George E. Kaattari, Jack N. Nielsen,
and William C. Pitts

SUMMARY

This report is the second in a series investigating the effects of interference at supersonic speeds on the aerodynamic properties of wing-body combinations. The first report, NACA RM A51J04, 1951, presented a method of determining the lift of triangular, rectangular, and trapezoidal wing-body combinations. The present report extends the same method to the determination of the pitching moments of these combinations. Calculated centers of pressure are compared with experimental values for nearly 100 triangular, rectangular, and trapezoidal wing-body combinations. The experimental and estimated locations of centers of pressure were found to correlate as follows: The correlation points for the triangular wing-body combinations have an average deviation of 0.008 body length about the line of best fit which is displaced 0.009 body length from the line of perfect agreement. The correlation points for the rectangular wing-body combinations have an average deviation of 0.015 body length about the line of best fit which is displaced 0.026 body length from the line of perfect agreement. The correlation points for the trapezoidal wing-body combinations have an average deviation of 0.016 body length about the line of best fit which is displaced 0.017 body length from the line of perfect agreement. It is recommended for design purposes that these displacements of the lines of best fit from the line of perfect agreement be subtracted from the appropriate theoretical value for center-of-pressure position. A numerical example illustrating the method is given.

INTRODUCTION

The first report of this series (reference 1) reviewed the existing methods of calculating lift components of wing-body combinations. These methods are either laborious or restricted to particular wing-body

[redacted]

combinations. In order to fill the need for a simple, general method applicable to a variety of combinations, a generalization of the method of Nielsen, Katzen, and Tang (reference 2) which successfully predicts the lift of triangular wing-body combinations is presented in reference 1. The applicability of the method has been verified by comparison with experimental results involving a wide variety of supersonic wing-body combinations including nearly 100 triangular, rectangular, and trapezoidal wing-body combinations. The present report extends reference 1 to include a method for calculation of the centers of pressure of the lift components of a wing-body combination and thus permits the calculation of the pitching moment of the combination.

SYMBOLS

A	aspect ratio of wing panels joined together
C_{L_α}	lift-curve slope based on exposed wing alone $\left(\frac{dL/d\alpha}{qS}\right)$
C_{M_α}	moment-curve slope based on exposed wing alone $\left(\frac{dM/d\alpha}{qS\bar{l}_r}\right)$
c_r	chord at wing-body juncture, inches
c_t	chord at wing tip, inches
c_y	wing chord at spanwise distance y from body axis, inches
d	body diameter, inches
$K_{B(W)}$	ratio of lift of body in presence of wing exclusive of nose to that of wing alone
K_N	ratio of lift of body nose to that of wing alone
$K_{W(B)}$	ratio of lift of wing in presence of body to lift of wing alone
L	lift force, pounds
l	body length, inches
l_a	body length behind wing trailing edge, inches
l_f	body length forward of wing leading edge, inches
$\bar{l}$	distance from most forward point of body to center of pressure, inches

$\bar{l}_M$	distance from most forward point of body to moment center of combination, inches
$\bar{l}_N$	distance from most forward point of body to center-of-pressure position of body nose, inches
$\bar{l}_r$	moment reference length, inches
M	moment, pound-inches
M_o	free-stream Mach number
m	cotangent of leading-edge sweep angle
q	free-stream dynamic pressure, pounds per square inch
r	body radius, inches
S	exposed wing area, square inches
s_m	semispan of wing-body combination, inches
V	volume of body considering the body as cylindrical behind the position of maximum cross section, cubic inches
x,y,z	streamwise, spanwise, and vertical coordinates, respectively
$\bar{x}$	chordwise distance from leading edge of wing-body juncture to center of pressure, inches
$\bar{x}_y$	chordwise distance from leading edge of wing-body juncture to local center of pressure at spanwise location y, inches
α_B	angle of attack of body
α_y	local angle of attack at spanwise distance y from body axis
β	$\sqrt{M_o^2 - 1}$
$\Lambda_{L.E.}$	leading-edge sweep angle
λ	taper ratio $\left(\frac{c_t}{c_r}\right)$

Subscripts

B	body alone
B(W)	body in presence of wing minus body nose

C	wing-body combination
C-N	combination minus nose
N	nose of combination
W	wing alone
W(B)	wing in presence of body

Superscripts

s	slender body
u	upwash theory

ANALYSIS

Since slender-body results are used in this analysis, the method is restricted to those wing-body combinations for which slender-body results are available. This means that at the present time swept-forward leading edges or swept-back trailing edges are generally precluded. A typical configuration is shown in figure 1, which gives the necessary dimensions required in lift and moment calculations.

The moment of a combination is the summation of the moments of all lift forces acting on the combination. To compute these moments requires that all lift forces and their locations (centers of pressure) be found. The methods of determining these forces and of finding their corresponding locations are now discussed.

Lift Components

The lift components of a combination are considered to be the lift of the body nose[1] L_N, the lift of the wing in presence of the body $L_{W(B)}$, and the additional lift of the body due to the presence of the wing (exclusive of the nose) $L_{B(W)}$. These components, following reference 1,

[1] The nose of the body is that part of the body in front of the wing leading-edge body juncture, or, in cases where the wing is mounted on an expanding body section, is that part of the body in front of the position of maximum cross section.

are conveniently evaluated by multiplying the lift of the wing alone (defined as the exposed wing panels joined together) by appropriate factors K_N, $K_{W(B)}$, and $K_{B(W)}$. Thus with $L_N = K_N L_W$, $L_{W(B)} = K_{W(B)} L$, and $L_{B(W)} = K_{B(W)} L_W$, the lift of the combination is given by

$$L_C = [K_N + K_{W(B)} + K_{B(W)}]L_W \tag{1}$$

where L_W may be either the theoretical or experimental value. The value for L_W calculated by linear theory is used throughout this report.

Evaluation of K_N.- The factor K_N is defined as

$$K_N = \frac{L_N}{L_W} \tag{2}$$

giving the ratio of nose lift to that of the wing alone. The lift of the nose in equation (2) may be evaluated by slender-body theory

$$\frac{L_N}{q\alpha} = 2\pi r^2 \tag{3}$$

The slender-body value for L_N was used in the present report and in reference 1. It is natural, however, to expect improved accuracy by using linear theory, and linear-theory results for L_N may be used if desired.

Evaluation of $K_{W(B)}$.- For lift of the wing in the presence of the body, the factor $K_{W(B)}$ is defined as follows:

$$K_{W(B)} = \frac{L_{W(B)}}{L_W} \tag{4}$$

It was shown in reference 1 that the ratio of the lift of a wing in combination with an infinite cylindrical body to that of wing alone as given by slender-body theory $K_{W(B)}{}^{(s)}$ is valid even for high aspect-ratio wings. The value of $K_{W(B)}{}^{(s)}$ is presented in figure 2 as a function of r/s_m and has been used for $K_{W(B)}$ in this report.

Evaluation of $K_{B(W)}$.- The method of determining the additional lift of the body due to the presence of the wing, as given in reference 1, is based on the concept of the body supporting lifting disturbances emanating from the wing. The region between the Mach helices on the

body originating at the wing leading and trailing edges, as shown in figure 3(a), represents the region supporting most of the lift carried over to the body from the wing. Simplification of this nonplanar model to the equivalent planar representation shown in figure 3(b) is desirable for purposes of calculation. The body is then represented by a flat plate at zero angle of attack ($\alpha_B = 0$) and the Mach helices of figure 3(a) become Mach lines in figure 3(b).

The value of lift carried over onto the body by a half wing with supersonic leading edge is given by

$$L = \frac{4q\alpha_W}{\beta\pi} \frac{\beta m}{\sqrt{\beta^2 m^2 - 1}} \int_0^d d\eta \int_\eta^{c_r+\eta} \cos^{-1} \frac{\frac{\xi}{\beta} + \beta m \eta}{\eta + m\xi} \, d\xi \tag{5}$$

with the coordinate system of figure 3(b). (See reference 1.) This result, doubled to account for the lift of two half wings and divided by the lift of the wing alone, gives $K_{B(W)}$.

$$K_{B(W)} = \frac{8\beta m}{\pi\sqrt{\beta^2 m^2 - 1}\,(1+\lambda)\left(\frac{\beta d}{c_r}\right)\left(\frac{s_m}{r} - 1\right)\left(\beta C_{L_\alpha}\right)_W}$$

$$\left\{ \left(\frac{\beta m}{\beta m+1}\right)\left[\frac{(\beta m+1)\frac{\beta d}{c_r} + \beta m}{\beta m}\right]^2 \cos^{-1}\left[\frac{1 + (1+\beta m)\beta\frac{d}{c_r}}{\beta m + (\beta m+1)\frac{\beta d}{c_r}}\right] + \right.$$

$$\frac{\sqrt{\beta^2 m^2 - 1}}{(\beta m+1)}\left(\sqrt{1+2\frac{\beta d}{c_r}} - 1\right) - \frac{\sqrt{\beta^2 m^2 - 1}}{\beta m}\left(\frac{\beta d}{c_r}\right)^2 \cosh^{-1}\left(1 + \frac{c_r}{\beta d}\right) -$$

$$\left. \frac{\beta m}{1+\beta m}\cos^{-1}\left(\frac{1}{\beta m}\right)\right\} \ldots \tag{6}$$

when $m\beta > 1$.

Similarly for subsonic edges there is obtained

$$L = \frac{8q\alpha_W(\beta m)^{3/2}}{\pi\beta(\beta m+1)}\int_0^d d\eta \int_\eta^{c_r+\eta} \frac{\sqrt{\frac{\xi}{\beta}-\eta}}{\sqrt{m\xi+\eta}}\, d\xi \quad . \; . \; . \tag{7}$$

giving

$$K_{B(W)} = \frac{16\frac{\beta^2 m^2}{(1+\beta m)^2}}{\pi(1+\lambda)\left(\frac{\beta d}{c_r}\right)\left(\frac{s_m}{r}-1\right)\left(\beta C_{L_\alpha}\right)_W}\left\{\left[\frac{\beta m + (1+\beta m)\frac{\beta d}{c_r}}{\beta m}\right]^{3/2} + \left[\frac{\beta m + (1+\beta m)\frac{\beta d}{c_r}}{\beta m}\right]^{1/2} - 2 - \left[\frac{(1+\beta m)\frac{\beta d}{c_r}}{\beta m}\right]^2 \tanh^{-1}\sqrt{\frac{\beta m}{\beta m + (1+\beta m)\frac{\beta d}{c_r}}}\right\} \; . \; . \; . \tag{8}$$

when $m\beta < 1$.

Tip effects are not considered and the analysis is confined to cases in which the Mach line from the leading edge of the wing tip falls behind the assumed region of lift carried over onto the body. This condition imposes the restriction

$$\beta A\,(1+\lambda)\left(\frac{1}{m\beta}+1\right) \geq 4 \tag{9}$$

on the wings for which equations (6) and (8) are to apply. Equations (6) and (8) are represented graphically by plotting the quantity

$$K_{B(W)}\,(1+\lambda)\left(\frac{s_m}{r}-1\right)\left(\beta C_{L_\alpha}\right)_W$$

as a function of $\beta d/c_r$ for constant values of $m\beta$ in figure 4, which is to serve as a design chart in determining $K_{B(W)}$ subject to the restriction of equation (9).

In reference 1, the following selection rule was given for choosing between $K_{B(W)}$ and $K_{B(W)}^{(s)}$: If $\beta A(1+\lambda)\left(\frac{1}{m\beta}+1\right) < 4$, use the slender-body value of $K_{B(W)}^{(s)}$ from figure 2. If $\beta A(1+\lambda)\left(\frac{1}{m\beta}+1\right) \geq 4$, use the

value of $K_{B(W)}$ given by figure 4 unless $K_{B(W)} > K_{B(W)}^{(s)}$. In such cases use $K_{B(W)}^{(s)}$.

Center of Pressure Positions

Center of pressure of the body nose.- The location of center of pressure of the body nose as given by slender-body theory is

$$\bar{l}_N = l\left(1 - \frac{V}{\pi r^2 l}\right) \tag{10}$$

where V is the volume of the body considering the body as cylindrical behind the position of maximum cross section. Equation (10) is used in this report, although the linear-theory result for $\bar{l}_N$, if available, may be expected to give improved accuracy.

Center of pressure of wing in presence of body.- Several methods of determining the center of pressure of a wing in the presence of a body will now be presented.

The center of pressure of a triangular wing in the presence of an infinite cylindrical body as given by slender-body theory (reference 3), in percent of the exposed wing root chord measured from the leading edge of the wing-body juncture, is

$$\left(\frac{\bar{x}}{c_r}\right)_{W(B)}^{(s)} = \frac{2\left(\frac{1}{3}+\frac{r^4}{s_m^4}\right)\tan^{-1}\left(\frac{s_m}{r}\right)+\frac{2}{3}\frac{r^3}{s_m^3}\ln\left[\left(\frac{s_m^2+r^2}{2s_m^2}\right)^2\frac{s_m}{r}\right]-\frac{1}{3}\frac{r^3}{s_m^3}\left(2\pi-1+\frac{s_m^2}{r^2}\right)}{\left(1-3\frac{r^2}{s_m^2}\right)\tan^{-1}\left(\frac{s_m}{r}\right)-\frac{r^2}{s_m^2}\left[\pi+\left(\frac{s_m}{r}-\frac{r}{s_m}\right)\right]} \tag{11}$$

An alternate method for evaluating center-of-pressure location of a triangular wing-body combination is to suppose that the exposed wings are operating in the upwash field of the body alone and then to calculate the resultant center-of-pressure location using strip theory. Neglecting any effect of the nose, it has been pointed out (reference 4)

that the upflow angle due to the body varies spanwise on the horizontal plane of symmetry as

$$\alpha_y = \alpha_B \left(1 + \frac{r^2}{y^2}\right) \tag{12}$$

where y is the lateral distance from the body axis. The wing is thus effectively twisted by the body-alone flow. If now the upwash angle given by equation (12) is taken into account by using strip theory, an approximate value of lift is given as

$$L_{W(B)}{}^{(u)} = \frac{4}{\beta} q \int_r^{s_m} \alpha_y \, c_y \, d_y \tag{13}$$

The moment about the leading edge of the root chord is

$$M_{W(B)}{}^{(u)} = \frac{4}{\beta} q \int_r^{s_m} \alpha_y \, \bar{x}_y \, c_y \, d_y \tag{14}$$

on the assumption that the center of pressure of the strip is at the midchord. Dividing moment by lift then gives for the center-of-pressure location for a triangular wing-body combination

$$\left(\frac{\bar{x}}{c_r}\right)_{W(B)}^{(u)} = \frac{1}{2} + \frac{\frac{1}{6} - \frac{1}{2}\frac{r}{s_m} - \frac{3}{2}\frac{r^2}{s_m{}^2} + \frac{11}{6}\frac{r^3}{s_m{}^3} + \left(1 + \frac{r}{s_m}\right)\frac{r^2}{s_m{}^2} \ln \frac{s_m}{r}}{2\left(1 - \frac{r}{s_m}\right)\left[\frac{1}{2}\left(1 - \frac{r^2}{s_m{}^2}\right) - \frac{r^2}{s_m{}^2} \ln \left(\frac{s_m}{r}\right)\right]} \tag{15}$$

The results of equations (11) and (15) are presented in figure 5 as a function of r/s_m. In addition, the value of center of pressure of the wing alone as determined by linear theory is indicated. It is significant that all three methods give essentially the same result for the center-of-pressure location of the wing in presence of the body. It may be concluded that $(\bar{x}/c_r)_W$ for wing alone (defined as exposed wing panels joined together), although independent of r/s_m, gives a sufficiently accurate representation of $(\bar{x}/c_r)_{W(B)}$ for triangular wings in presence of the body.

If slender-body theory is applied to rectangular wings in combination, the erroneous result is obtained that all lift, and therefore the center of pressure, is at the wing leading edge. While this result is valid for vanishing aspect ratio, it is obviously not valid in general. On the other hand, by strip theory, the center of pressure is given at

the midchord and is independent of the aspect ratio. This value is exact only in the case of vanishing chord and is approximately true for moderate to high aspect ratios. The center-of-pressure location of wing alone as predicted by linear theory exhibits a shift toward the leading edge from the midchord position with decreasing aspect ratio.

$$\left(\frac{\bar{x}}{c_r}\right)_W = \frac{3\beta A-2}{6\beta A-3} \quad . \; . \; . \tag{16}$$

Equation (16) is valid for $\beta A \geq 1$. For $\beta A < 1$, negative lifting pressures due to tip effects develop on rearward areas of the wing, moving the center of pressure nearer the wing leading edge. Thus, wing-alone center-of-pressure location as predicted by linear theory approaches the value given by strip theory for wings (in presence of body) of high aspect ratios and shows a location more in accordance with slender-body-theory results at low aspect ratios. It is therefore concluded that the center of pressure of the wing alone for all aspect ratios is more representative of the center of pressure of the lift on the wing in presence of a body than the result given by either slender-body theory or strip theory.

For trapezoidal wings of no trailing-edge sweep, slender-body theory gives all the lift, and hence center of pressure, on the portions of the wing forward of the leading edge of the tip chord. In general, however, lift is known to exist over the entire wing and the slender-body result for center-of-pressure location is too far forward at high aspect ratios. Strip theory, on the other hand, principally by not accounting for tip effects, generally gives a center-of-pressure location too far aft of the wing leading edge particularly at low aspect ratios. For large aspect ratios wing-alone theory is in good accord with strip theory, and at low aspect ratios, with slender-body theory. Since strip theory is reliable only at high aspect ratios, it can be concluded that wing-alone theory is best for the entire aspect-ratio range.

On the basis of the foregoing comparison of wing-alone theory with slender-body theory and strip theory for triangular, rectangular, and trapezoidal wings in combination with a body, it is concluded that of these three theories wing-alone theory is the best for representing the center of pressure of the exposed wing panels throughout the aspect-ratio range. Some simple charts to assist in estimating these center-of-pressure positions are now presented.

Figures 6(a), 6(b), and 6(c) give the variation of $(\bar{x}/c_r)_W$ with βA for wings of no trailing-edge sweep, no midchord sweep, and no leading-edge sweep, respectively, for taper ratios of $\lambda = 0$, 1/2, and 1. The curves giving $(\bar{x}/c_r)_W$ are extrapolated to the limiting values given by slender-body theory at $\beta A = 0$, for which case

slender-body theory is valid. Figures 6(a), 6(b), and 6(c) serve as design charts, and the value of $(\bar{x}/c_r)_{W(B)}$ for any given wing of this family may be found by suitable interpolation. If more accurate results are available for the wing-alone center of pressure, these results may be used instead of those found from figure 6.

Center of pressure of lift on body due to the wing.- The method of determining center-of-pressure location of the lift on the body due to the wing is based on the same model used to determine the lift in reference 1. (See fig. 3.) The moment of the lift (equation (5)) carried onto the body by a wing with a supersonic leading edge is

$$M_{B(W)} = \frac{4q\alpha_W\beta m}{\beta^2\pi\sqrt{\beta^2m^2-1}}\int_0^d d\eta\int_\eta^{c_r+\eta} \xi \cos^{-1}\frac{\frac{\xi}{\beta}+\beta m\eta}{\eta+m\xi}\,d\xi \tag{17}$$

with the coordinate system of figure 3(b). This result, doubled to account for the lift of two half-wings, gives

$$M_{B(W)} = \frac{4q\alpha_W m\beta}{3\pi}c_r^3\left\{\sqrt{1+\frac{2\beta d}{c_r}}\left[\frac{2m\beta+5}{3(m\beta+1)^2}+\frac{\beta d/c_r}{3(m\beta+1)}-\frac{(\beta d/c_r)^2}{\beta m}\right]+\right.$$

$$\frac{1}{\sqrt{m^2\beta^2-1}}\left[\left(1+\frac{\beta d}{c_r}\right)^3-\frac{(\beta d/c_r)^3}{m^2\beta^2}-\frac{1}{(1+m\beta)^2}\right]\cos^{-1}\left[\frac{1+\frac{\beta d}{c_r}(m\beta+1)}{m\beta+\frac{\beta d}{c_r}(m\beta+1)}\right]+$$

$$\left.\left(\frac{\beta d}{c_r}\right)^3\frac{1}{m^2\beta^2}\cosh^{-1}\left(1+\frac{c_r}{\beta d}\right)-\left[\frac{2m\beta+5}{3(m\beta+1)^2}\right]-\frac{\left[1-\left(\frac{1}{m\beta+1}\right)^2\right]}{\sqrt{m^2\beta^2-1}}\cos^{-1}\frac{1}{m\beta}\right\} \tag{18}$$

The center-of-pressure location is then found using $K_{B(W)}$ from equation (6) and the moment from equation (18) as follows:

$$\left(\frac{\bar{x}}{c_r}\right)_{B(W)} = \frac{M_{B(W)}}{L_{B(W)}c_r} = \frac{M_{B(W)}}{K_{B(W)}L_W c_r} \tag{19}$$

Similarly for wings with subsonic edges there is obtained

$$M_{B(W)} = \frac{8q\alpha_W(m\beta)^{3/2}}{\pi\beta^2(\beta m+1)}\int_0^d d\eta \int_\eta^{c_r+\eta} \frac{\xi\sqrt{\frac{\xi}{\beta}-\eta}}{\sqrt{m\xi+\eta}}\,d\xi \tag{20}$$

giving

$$M_{B(W)} = \frac{4q\alpha_W}{\pi}c_r^3\left\{\frac{\sqrt{m^2\beta^2+m\beta(m\beta+1)\frac{\beta d}{c_r}}}{9m\beta(m\beta+1)^3}\left[(8m\beta+24)m^2\beta^2+(14m\beta+6)m\beta\frac{\beta d}{c_r}+\right.\right.$$

$$\left.\left.3(m\beta-3)(m\beta+1)^2\left(\frac{\beta d}{c_r}\right)^2\right]-\frac{(8m\beta+24)m^3\beta^3}{9m\beta(m\beta+1)^3}-\frac{(m\beta-3)}{3m\beta}\left(\frac{\beta d}{c_r}\right)^3\cosh^{-1}\sqrt{\frac{m\beta+(m\beta+1)\frac{\beta d}{c_r}}{(m\beta+1)\frac{\beta d}{c_r}}}\right\} \tag{21}$$

The moment of equation (21) with $K_{B(W)}$ of equation (8) is used in equation (19) to give the center of pressure of the lift on an infinite cylindrical body due to the wing. The results for center of pressure for both supersonic and subsonic cases are presented as a function of $\beta d/c_r$ with $m\beta$ as the parameter in figure 7, which is to serve as a design chart. It is notable that the effect of $m\beta$ is small.

According to the results of slender-body theory, the location of the center of pressure of the body in presence of the wing measured aft of the leading edge of the wing-body juncture is

$$\left(\frac{\bar{x}}{c_r}\right)^{(s)}_{B(W)} = \frac{K_{W(B)}{}^{(s)} + K_{B(W)}{}^{(s)}}{\left(1-\frac{r}{s_m}\right)K_{B(W)}{}^{(s)}}\left[\frac{2}{3}+\frac{4}{3}\left(\frac{\frac{r}{s_m}}{1+\frac{r}{s_m}}\right)^2-\frac{r}{s_m}\right]-$$

$$\frac{K_{W(B)}{}^{(s)}}{K_{B(W)}{}^{(s)}}\left(\frac{\bar{x}}{c_r}\right)^{(s)}_{W(B)} \tag{22}$$

where $K_{B(W)}{}^{(s)}$ and $K_{W(B)}{}^{(s)}$ are functions of r/s_m (fig. 2) and $\left(\frac{\bar{x}}{c_r}\right)^{(s)}_{W(B)}$ is given by equation (11). Equation (22) is also plotted

against $\beta d/c_r$ with $m\beta$ as the parameter in figure 7 for comparison with the previous analysis. Again, $m\beta$ is seen to have no large effect on the center of pressure. The slender-body value of $\left(\frac{\bar{x}}{c_r}\right)^{(s)}_{B(W)}$ is seen to begin at a value of 0.5 for $\beta d/c_r = 0$ in agreement with the results of the previous analysis. However, for increasing values of $\beta d/c_r$ the slender-body results show an asymptotic maximum of $\left(\frac{\bar{x}}{c_r}\right)^{(s)}_{B(W)} = \frac{2}{3}$; whereas by the previous analysis, which accounts for afterbody, the value of $\left(\frac{\bar{x}}{c_r}\right)_{B(W)}$ continually increases with $\frac{\beta d}{c_r}$. The latter result is to be anticipated by a consideration of figure 3(a). For a given geometry, an increase in Mach number causes a primary portion of the pressure disturbance carried onto the body to sweep beyond the wing trailing edge. Similarly, a decrease in chord with a given Mach number and body diameter moves the wing trailing edge ahead of the primary portion of the lift disturbance carried onto the body. In view of the foregoing arguments and since slender-body theory does not properly account for an afterbody, the present method of determining $\left(\frac{\bar{x}}{c_r}\right)_{B(W)}$ is applied to combinations with afterbodies. Figure 7 serves as a design chart for all wing-body combinations with afterbodies.

Center of pressure of the combination.- The center-of-pressure location of a complete configuration in terms of body length is given by

$$\left(\frac{\bar{l}}{l}\right)_C = \frac{K_N\bar{l}_N + K_{W(B)}\bar{l}_{W(B)} + K_{B(W)}\bar{l}_{B(W)}}{l[K_N + K_{W(B)} + K_{B(W)}]} \tag{23}$$

where $\bar{l}_N$ is given by equation (10) and

$$\bar{l}_{W(B)} = l_f + \left(\frac{\bar{x}}{c_r}\right)_{W(B)} c_r \tag{24}$$

$$\bar{l}_{B(W)} = l_f + \left(\frac{\bar{x}}{c_r}\right)_{B(W)} c_r \tag{25}$$

NUMERICAL EXAMPLE

To illustrate the use of the method developed in the foregoing sections, the determination of the center-of-pressure location of a trapezoidal wing-body combination is now presented. Given that $c_t = 1.500$, $c_r = 3.878$, $r = 0.850$, $s_m = 3.790$, $M_o = 2.87$, $l_f = 16.06$, $l = 24.00$, $V = 39.96$ and no midchord sweep, the basic parameters may be evaluated as follows:

$$A = \frac{4(2.940)}{1.5 + 3.878} = 2.19, \text{ aspect ratio of the wing alone}$$

$$\beta = \sqrt{M_o^2-1} = \sqrt{2.87^2-1} = 2.69$$

$$\beta A = 5.89, \text{ effective aspect ratio}$$

$$r/s_m = 0.224 \text{ body radius, semispan ratio}$$

$$\lambda = \frac{1.500}{3.878} = 0.387 \text{ taper ratio}$$

$$m = \frac{2(2.94)}{3.878 - 1.5} = 2.47$$

$$m\beta = 6.64$$

$$\frac{\beta d}{c_r} = \frac{(2.69)(1.7)}{3.878} = 1.18$$

The value of $\beta\left(C_{L_\alpha}\right)_W$ from the charts of reference 5 is 3.85. The value of the parameter in equation (9) is

$$\beta A(1+\lambda)\left(\frac{1}{m\beta} + 1\right) = (5.89)(1.387)\left(\frac{1}{6.64} + 1\right) > 4$$

The preceding information now enables the lift parameters in equation (23) to be determined as follows:

K_N given by equations (2) and (3) is

$$K_N = \frac{2\pi r^2}{(s_m-r)(c_r+c_t)\left(\beta C_{L_\alpha}\right)/\beta} = \frac{2\pi(0.85)^2}{2.94(1.50 + 3.878)(3.85)/2.69} = 0.200$$

$K_{W(B)}{}^{(s)}$ from figure 3, for $r/s_m = 0.224$, is

$$K_{W(B)} = 1.18$$

$K_{B(W)}$ from figure 4 in parametric form is

$$K_{B(W)} \left(\beta C_{L_\alpha}\right)_W (1 + \lambda) \left(\frac{s_m}{r} - 1\right) = 4.41$$

The value of $K_{B(W)}$ is thus

$$K_{B(W)} = \frac{4.41}{(3.85)(1.387)(3.46)} = 0.24$$

Now determine $K_{B(W)}{}^{(s)}$ from figure 2:

$$K_{B(W)}{}^{(s)} = 0.31$$

Since $K_{B(W)} < K_{B(W)}{}^{(s)}$, the value of $K_{B(W)}$ is to be used.

The remaining parameters $\bar{l}_N$, $\bar{l}_{W(B)}$, and $\bar{l}_{B(W)}$ are obtained in the following manner:

$\bar{l}_N$ from equation (10) is

$$\bar{l}_N = l\left(1 - \frac{V}{\pi r^2 l}\right) = 24\left[1 - \frac{39.96}{\pi(0.85)^2(24)}\right] = 6.4$$

$\bar{l}_{W(B)}$ from equation (24) is

$$\bar{l}_{W(B)} = l_f + \left(\frac{\bar{x}}{c_r}\right)_{W(B)} c_r = 16.06 + (0.49)(3.787) = 17.96$$

where the value of $\left(\frac{\bar{x}}{c_r}\right)_{W(B)} = 0.49$ was obtained by interpolation from figure 6(b).

$\bar{l}_{B(W)}$ from equation (25) is

$$\bar{l}_{B(W)} = l_f + \left(\frac{\bar{x}}{c_r}\right)_{B(W)} c_r = 16.06 + (1.08)(3.878) = 20.25$$

where the value for $\left(\frac{\bar{x}}{c_r}\right)_{B(W)}$, from figure 7, is 1.08.

[redacted]

The distance to the center of pressure of the combination from the most forward point of the body is then given by

$$\left(\frac{\bar{l}}{l}\right)_C = \frac{K_N\bar{l}_N + K_{W(B)}\bar{l}_{W(B)} + K_{B(W)}\bar{l}_{B(W)}}{l\left[K_N + K_{W(B)} + K_{B(W)}\right]} \quad . \; . \; . \tag{23}$$

$$= \frac{(0.200)(6.4) + (1.18)(17.96) + (0.24)(20.25)}{24\ (0.200 + 1.18 + 0.24)} = 0.702$$

EXPERIMENTAL VERIFICATION

The foregoing analysis has been applied to the calculation of the centers of pressure of nearly 100 wing-body combinations of widely varying plan form. The results are compared with the experimental center of pressure found by putting the experimental values of C_{L_α} and C_{M_α} into the expression

$$\left(\frac{\bar{l}}{l}\right)_C = \frac{\bar{l}_M - \left(C_{M_\alpha}/C_{L_\alpha}\right)\bar{l}_r}{l} \quad . \; . \; . \tag{26}$$

where $\bar{l}_r$ is the moment reference length in inches. Tables I, II, and III summarize the experimental and calculated centers of pressure for the triangular, rectangular, and trapezoidal wing-body combinations and also give the theoretical centers of pressure for the lift of the body nose, the lift of the wing in presence of the body, and of the additional lift on the body due to the presence of the wing. The correlation between the experimental and estimated results for the triangular, rectangular, and trapezoidal wing-body combinations are shown in figures 8, 9, and 10, respectively.

The sources of the test data are listed in references 6 to 27; some of the test data are unpublished. Some difficulty was met in trying to determine values of lift- and moment-curve slopes from published curves because of irregularities in the data. In such cases the average values of C_{M_α} and C_{L_α} over a small angle-of-attack range about $\alpha = 0$ were used. Furthermore, some experimental lift and moment-curve slopes were questionable. In one case, data on similar configurations from different facilities (of different Reynolds numbers) gave a difference of the order of 10 percent in the lift-curve slopes. In view of the foregoing, some of the deviation found in the correlations of experimental and calculated center-of-pressure positions can be ascribed to questionable experimental data.

Since the division of lift and moment between wing and body was not given by experiment, comparison with the method for center of pressure for the lift of the body nose, the lift of the wing in presence of body, and the additional lift on the body in presence of the wing could not be made directly. The correlation was therefore made on the basis of center of pressure of the entire combination.

Triangular Wing-Body Combinations

The correlation of estimated center-of-pressure positions with those of experiment for triangular wing-body combinations is presented in figure 8. Included in figure 8 is a line of perfect agreement and also lines of $\pm 0.05\ l$ deviation from perfect agreement. The correlation of estimated values with those of experiment is excellent; the line of mean correlation is displaced 0.009 body length from the line of perfect agreement and the average deviation from the mean is only 0.008 body length.

Rectangular Wing-Body Combinations

The correlation of estimated center-of-pressure positions with those of experiment for rectangular wing-body combinations is presented in figure 9. The correlation of estimated values with those of experiment is not so good as that for triangular wing-body combinations. The line of mean correlation is displaced about 0.026 body length from the line of perfect agreement. The average deviation from the mean is 0.015 body length. A possible effect that can explain the difference in correlation between the triangular and rectangular wing-body combinations is that due to the wing tip. It may be seen that the lift carry-over from a rectangular wing onto the shaded area of the body shown in figure 3(b) is independent of span, provided that $\beta A \geq 2$, and may be considered that due to an infinite wing. In order to form a finite wing, a "canceling wing" must be superposed on the infinite wing to form a wing tip. This canceling wing generates a negative lift which carries over in part onto the body aft of the trailing edge of the wing at a distance which depends primarily on the Mach number and wing semispan. While this negative lift carry-over is probably small, its effect on the over-all moment and center-of-pressure position of the combination may be appreciable due to the large moment arm involved. Since no account was taken of this decreased lift on the afterbody, the calculated centers of pressure for the rectangular wing-body combinations are too far aft. Triangular wings, having no tip chord, may be expected to have less wing-tip effects than rectangular wings.

Trapezoidal Wing-Body Combinations

The correlation of estimated center-of-pressure positions with those of experiment for trapezoidal wing-body combinations is presented in figure 10. Correlation of estimated values with those of experiment is generally within the $\pm 0.05\ l$ correlation limits excluding the combinations with no afterbody. The line of mean correlation is displaced 0.017 body length from perfect agreement and the average deviation from the mean is 0.016 body length. It is notable that the mean displacement from correlation for trapezoidal wing-body combinations is intermediate between those of triangular and rectangular wing-body combinations as might be surmised.

Combinations With No Afterbody

The present equations are applicable only to those combinations having an afterbody. However, as a matter of interest, some combinations with no afterbody, the centers of pressure of which were computed on the basis of having an afterbody, are presented in figures 8, 9, and 10 (denoted by flagged symbols). A sufficient number is not included for each type of combination to make a reliable statistical comparison. However, on the whole these combinations show a somewhat greater mean displacement of the line of best fit from the line of perfect agreement than do combinations with an afterbody, indicating that an afterbody has an appreciable effect.

DISCUSSION

The question arises how large an error can be made by neglecting interference in determining the center of pressure of a combination. The answer depends on how the components of the combination are added together neglecting interference. First, the combination may be assumed to act as the sum of the body alone plus the exposed wings joined together. On the other hand, the combination may be considered as the sum of the body alone and the entire wing where the entire wing is formed by the extension of the wing leading and trailing edges to the body center line. For the rectangular wing-body combinations considered, estimating the center-of-pressure positions using either approach gives as good a correlation as is given by the present method. For triangular wing-body combinations the center-of-pressure locations computed on the basis of the exposed wing, neglecting interference, do not correlate as well as those computed by the present method. The correlation scatters from near agreement up to values of about 20 percent of the body length

forward of the experimental values. The scatter of the correlation points becomes even greater when the center of pressure is computed on the basis of the entire wing. For trapezoidal wing-body combinations, a better correlation is attained than in the case of triangular wings; however, the correlation by either approach is not so good as with the present method showing a greater scatter about the line of best fit, and, in general, giving center-of-pressure positions too far forward on the combinations.

It is recommended that the present method be used for calculating the pitching moment of a combination for the following reasons: First, the present method is rational and is applicable to a variety of wing-body combinations. Second, both the center-of-pressure position and the lift are provided in determining the pitching moment of a combination. Third, the breakdown of the combination moment into its components is given.

For purposes of calculation, it is recommended that the appropriate displacement value of the line of best fit from the line of perfect agreement be applied as a correction in determining the center-of-pressure position of a combination by subtracting it from the center-of-pressure position given by theory. When this correction is applied, an average deviation of 0.016 body length or less, depending on the wing plan form, may be expected in the location of center-of-pressure position. The uncertainty in the center-of-pressure position in terms of the wing mean aerodynamic chord is, of course, larger and depends on the ratio of body length to mean aerodynamic chord.

CONCLUSIONS

On the basis of the correlations between the estimated and experimental center-of-pressure locations presented for nearly 100 triangular, rectangular, and trapezoidal wing-body, Mach wave configurations, it was found that by the method of this report the following limits of correlation were attained: The correlation points for the triangular wing-body combinations have an average deviation of 0.008 body length about the line of best fit which is displaced 0.009 body length from the line of perfect agreement. The correlation points for the rectangular wing-body combinations have an average deviation of 0.015 body length about the line of best fit which is displaced 0.026 body length from the line of perfect agreement. The correlation points for the trapezoidal wing-body combinations have an average deviation of 0.016 body length about the line of best fit which is displaced 0.017 body length from the line of perfect agreement. It is recommended for design purposes that the displacement of the line of best fit from the line of perfect agreement be

subtracted from the appropriate theoretical value for center-of-pressure position.

Ames Aeronautical Laboratory
National Advisory Committee for Aeronautics
Moffett Field, Calif.

REFERENCES

1. Nielsen, Jack N., and Kaattari, George E.: Method for Estimating Lift Interference of Wing-Body Combinations at Supersonic Speeds. NACA RM A51J04, 1951.

2. Nielsen, Jack N., Katzen, Elliot D., and Tang, Kenneth K.: Lift and Pitching-Moment Interference Between a Pointed Cylindrical Body and Triangular Wings of Various Aspect Ratios at Mach Numbers of 1.50 and 2.02. NACA RM A50F06, 1950.

3. Spreiter, John R.: The Aerodynamic Forces on Slender Wing-Body Plane- and Cruciform-Wing and Body Combinations. NACA Rep. 962, 1950. (Formerly NACA TN's 1662 and 1897)

4. Beskin, Leon: Determination of Upwash Around a Body of Revolution at Supersonic Velocities. Johns Hopkins University, A.P.L. CM-251, 1946.

5. Lapin, Ellis: Charts for the Computation of Lift and Drag of Finite Wings at Supersonic Speeds. Douglas Aircraft Company, Inc., SM-13480, Oct. 1949.

6. Spahr, Richard J., and Robinson, Robert A.: Wind-Tunnel Investigation at Mach Numbers of 1.5 and 2.0 of a Canard Missile Configuration. NACA RM A51C08, 1951.

7. Jevon, R. W.: Data Report for Supersonic Wind Tunnel Tests on XSSM-N-6 Models #3C and #6A, 5th Dangerfield Test Period, M = 2.0. Grumman Aircraft Engineering Corporation, Rep. No. 3147.20, March 1950.

8. Jevon, R. W., and Bastedo, W., Jr.: Data Report for Supersonic Wind Tunnel Tests on XSSM-N-6 Model #3A, 1st Dangerfield Test Period, M = 2.0. Grumman Aircraft Engineering Corporation, Rep. No. P/A 3128.20, Apr. 1949.

9. Jevon, R. W.: Data Report for Supersonic Wind Tunnel Tests on XSSM-N-6 Models #3B and #4A, 2d-4th Dangerfield Test Periods, M = 2.0, 2.25, 1.73. Grumman Aircraft Engineering Corporation, Rep. No. P/A 3141.20, Sept. 1949.

10. Bastedo, W., Jr.: Data Report for Supersonic Wind Tunnel Tests on XSSM-N-6 Model #6, 2d Aberdeen Test Period, M = 1.72. Grumman Aircraft Engineering Corp., Rep. No. P/A 3107.21, July 1949.

11. Katzen, Elliott D., and Kaattari, George E.: Drag Interference Between a Pointed Cylindrical Body and Triangular Wings of Various Aspect Ratios at Mach Numbers of 1.50 and 2.02. NACA RM A51C27, 1951.

12. Peters, R. G.: Data Report for Supersonic Wind Tunnel Tests on GAPA Model FR-8, 6th and 7th Aberdeen Test Periods, M = 1.72 and M = 1.28. Boeing Airplane Co., D-8788 (Tech. Rep. 111-9), Feb. 1948.

13. Peters, R. G.: Data Report for Supersonic Wind Tunnel Tests on GAPA Model FR-8, 5th Aberdeen Test Period, M = 1.72. Boeing Aircraft Co., D-8397, (Tech. Rep. 111-7), Aug. 1947.

14. Rainey, Robert W.: Langley 9-Inch Supersonic Tunnel Tests of Several Modifications of a Supersonic Missile Having Tandem Cruciform Lifting Surfaces. Three-Component Data Results of Models Having Ratios of Wing Span to Tail Span Equal to 1. NACA RM L9L30, 1951.

15. Rainey, Robert W.: Langley 9-Inch Supersonic Tunnel Tests of Several Modifications of a Supersonic Missile Having Tandem Cruciform Lifting Surfaces. Three-Component Data Results of Models Having Ratios of Wing Span to Tail Span Less Than 1. NACA RM L50I29a, 1951.

16. Rainey, Robert W.: Langley 9-Inch Supersonic Tunnel Tests of Several Modifications of a Supersonic Missile Having Tandem Cruciform Lifting Surfaces. Three-Component Data Results of Models Having Ratios of Wing Span to Tail Span Equal to and Less Than 1 and Some Static Rolling-Moment Data. NACA RM L50G07, 1951.

17. Speth, Robert F.: Results of Rascal Supersonic Wind Tunnel Tests at M = 1.72. Bell Aircraft Corp. Rep. No. 56-980-001, Vol. 1, Dec. 1948.

18. Speth, Robert F.: Results of Rascal Supersonic Wind Tunnel Tests at M = 1.28. Bell Aircraft Corp. Rep. No. 56-980-001, Vol. 2, Dec. 1948.

19. Harshman, J., and Uddenberg, R. C.: Supersonic Wind Tunnel Tests of GAPA Models at a Mach Number of 1.28 in the Aberdeen Tunnel. Boeing Aircraft Co., Document No. D-7817, Aug. 2, 1946.

20. Uddenberg, R. C.: Supersonic Wind Tunnel Tests of GAPA Models at a Mach Number of 1.72 in the Aberdeen Tunnel. Boeing Aircraft Co., Document No. D-7818, Dec. 1946.

21. Flake, H. M.: Supersonic Wind Tunnel Tests of a 0.020-Scale Model of the NA-705 Missile at Mach Number 2.87 to Determine Effect of Aspect Ratio and Planform of Wings on the Aerodynamic Characteristics of Wing Plus Body. North American Aviation Inc., Rep. No. AL-1156, Oct. 1950.

22. Hall, Albert W., and Morris, Garland J.: Aerodynamic Characteristics at a Mach Number of 1.25 of a 6-Percent-Thick Triangular Wing and 6- and 9-Percent-Thick Triangular Wings in Combination With a Fuselage-Wing Aspect Ratio 2.31, Biconvex Airfoil Sections. NACA RM L50D05, 1950.

23. Fischer, H.S.: Supersonic Wind-Tunnel Tests of a 0.075-Scale Model of the Nike 482 Missile. Douglas Aircraft Co., Inc., SM-13848, Nov. 1950.

24. Grigsby, Carl E.: Investigation at a Mach Number of 1.93 to Determine Lift, Drag, Pitching Moment, and Average Downwash Characteristics for Several Missile Configurations Having Rectangular Wings and Tails of Various Spans. NACA RM L50I08, 1950.

25. Ellis, Macon C., Jr., and Grigsby, Carl E.: Aerodynamic Investigation at Mach Number 1.92 of a Rectangular Wing and Tail and Body Configuration and Its Components. NACA RM L9L28a, 1950.

26. Jaeger, B. F., and Brown, A. E.: The Aerodynamic Characteristics at Mach Number 2.0 of 14- and 18-Caliber Fin-Stabilized Rockets with Varying Body and Fin Parameters. U. S. Naval Ordnance Test Station, Inyokern, Calif. NAVORD Rep. 1211, Jan. 1950.

27. Dorrance, W. H.: Body-Tail Interference in Supersonic Flow Including an Example Application. University of Michigan, UMM-38, Aug. 1949.

[redacted]

TABLE I.- SUMMARY OF AERODYNAMIC AND GEOMETRIC CHARACTERISTICS AND TEST CONDITIONS FOR TRIANGULAR WING BODY COMBINATIONS

No.	Sketch	M_o	R	Wing section	$\bar{c}$ (in.)	βA	$\Lambda_{L.E.}$ (deg)	$\frac{r}{S_m}$	$\frac{l_a}{r}$	$\frac{l_f}{r}$	Reference	Facility
1		1.5	1.0×10^6	[1]d.w.	2	0.75	80.4	0.600	4	6.7	2	Ames 1x3 ft
2		2.0	1.0×10^6	d.w.	2	1.16	80.4	.600	4	6.7	2	Ames 1x3 ft
3		1.5	1.0×10^6	d.w.	2	1.50	71.6	.428	4	6.7	2	Ames 1x3 ft
4		2.0	1.0×10^6	d.w.	2	2.32	71.6	.428	4	6.7	2	Ames 1x3 ft
5		1.5	1.0×10^6	d.w.	2	2.26	63.2	.333	4	6.7	2	Ames 1x3 ft
6		2.0	1.0×10^6	d.w.	2	3.50	63.2	.333	4	6.7	2	Ames 1x3 ft
7		1.5	1.0×10^6	d.w.	2	3.01	56.0	.272	4	6.7	2	Ames 1x3 ft
8		2.0	1.0×10^6	d.w.	2	4.66	56.0	.272	4	6.7	2	Ames 1x3 ft
9		1.5	1.0×10^6	d.w.	2	3.72	50.3	.231	4	6.7	2	Ames 1x3 ft
10		2.0	1.0×10^6	d.w.	2	5.77	50.3	.231	4	6.7	2	Ames 1x3 ft
11		1.5	1.0×10^6	d.w.	2	4.47	45.0	.201	4	6.7	2	Ames 1x3 ft
12		2.0	1.0×10^6	d.w.	2	6.93	45.0	.201	4	6.7	2	Ames 1x3 ft
13		1.72	1.24×10^6	d.w.	3	1.50	75	.272	8.2	24.2	23	Aberdeen
14		1.25	$.88\times10^6$	[2]b.c.	3.51	1.73	60	.163	6.1	9.1	22	Langley 9 in.
15		1.28	1.11×10^6	d.w.	2.57	1.89	59.4	.215	7.7	10.1	19	Aberdeen
16		1.72	1.11×10^6	d.w.	2.57	3.31	59.4	.215	7.7	10.1	20	Aberdeen
17		2.87	$.56\times10^6$	d.w.	2.65	10.76	45	.176	5.5	18.0	21	NAA 16 in.
18	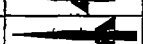	2.87	$.56\times10^6$	d.w.	2.65	10.76	0	.176	3.9	19.6	21	NAA 16 in.
19		2.87	$.74\times10^6$	d.w.	3.49	6.20	60	.220	5.0	17.1	21	NAA 16 in.
20		2.87	$.74\times10^6$	d.w.	3.49	6.20	0	.220	3.0	19.1	21	NAA 16 in.
21	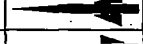	2.87	1.11×10^6	d.w.	5.12	2.88	75	.292	4.1	15.2	21	NAA 16 in.
22	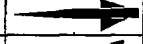	2.87	1.11×10^6	d.w.	5.12	2.88	0	.292	1.0	18.2	21	NAA 16 in.
23		1.15	1.26×10^6	d.w.	7.54	1.31	60	.216	13.9	11.6		Ames 6x6 ft
24	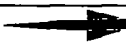	1.2	1.26×10^6	d.w.	7.54	1.53	60	.216	13.9	11.6		Ames 6x6 ft
25		1.3	1.26×10^6	d.w.	7.54	1.92	60	.216	13.9	11.6		Ames 6x6 ft
26		1.4	1.26×10^6	d.w.	7.54	2.26	60	.216	13.9	11.6		Ames 6x6 ft
27		1.53	1.26×10^6	d.w.	7.54	2.68	60	.216	13.9	11.6		Ames 6x6 ft
28		1.7	1.26×10^6	d.w.	7.54	3.18	60	.216	13.9	11.6		Ames 6x6 ft
29		1.2	$.59\times10^6$	d.w.	3.53	2.66	45	.254	0	28.9		Ames 6x6 ft
30	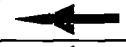	1.4	$.59\times10^6$	d.w.	3.53	3.92	45	.254	0	28.9		Ames 6x6 ft
31		1.7	$.59\times10^6$	d.w.	3.53	5.50	45	.254	0	28.9		Ames 6x6 ft
32		1.93	$.20\times10^6$	[3]hex.	.65	3.81	60	.382	12.1	10.1		Langley 9 in.
33	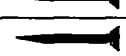	1.62	$.23\times10^6$	hex.	.65	2.94	60	.382	12.1	10.1		Langley 9 in.

[1]d.w. indicates double wedge.
[2]b.c. indicates biconvex.
[3]hex. indicates hexagonal.

TABLE I.- CONCLUDED

No.	$\beta A(1+\lambda)(\frac{1}{m_H}+1)$	K_H	K_B	$K_W^{(z)}$	Theoretical									Experimental			
					Lift			Center of pressure						Lift		Center of pressure	
					$\beta(C_{L_\alpha})_W$	$\beta(C_{L_\alpha})_H$	$\beta(C_{L_\alpha})_c$	$\bar{l}_H$	$\bar{l}_{W(B)}$	$\bar{l}_{B(W)}$	$\bar{l}_c$	$(\bar{l}/l)_c$	$(\bar{l}/d)_c$	$\beta(C_{L_\alpha})_B$	$\beta(C_{L_\alpha})_c$	$(\bar{l}/l)_c$	$(\bar{l}/d)_c$
1	4.7	2.33	0.97	1.56	1.13	2.63	5.48	2.09	7.00	7.42	4.73	0.43	3.15	2.56	6.35	0.44	3.22
2	5.1	2.44	.94	1.56	1.67	4.08	8.25	2.09	7.00	7.81	4.73	.43	3.15	5.38	10.02	.41	3.03
3	5.5	.64	.60	1.38	2.07	1.32	5.41	2.09	7.00	7.42	5.90	.54	3.93	1.29	5.86	.53	3.92
4	6.3	.71	.52	1.38	2.88	2.04	7.52	2.09	7.00	7.81	5.83	.53	3.88	2.69	8.33	.53	3.89
5	6.3	.31	.41	1.29	2.83	.88	5.69	2.09	7.00	7.42	6.33	.57	4.22	.86	5.77	.56	4.13
6	7.5	.36	.37	1.29	3.73	1.36	7.54	2.09	7.00	7.82	6.27	.57	4.18	1.79	8.24	.57	4.15
7	7.0	.19	.32	1.23	3.42	.66	5.95	2.09	7.00	7.42	6.53	.59	4.35	.64	5.71	.58	4.25
8	8.7	.26	.30	1.23	4.00	1.02	7.14	2.09	7.00	7.82	6.44	.58	4.29	1.35	7.76	.58	4.28
9	7.7	.14	.26	1.19	3.86	.53	6.13	2.09	7.00	7.42	6.64	.60	4.43	.52	5.69	.60	4.36
10	9.8	.20	.26	1.19	4.00	.82	6.62	2.09	7.00	7.82	6.52	.59	4.35	1.08	7.55	.60	4.36
11	8.5	.11	.23	1.16	4.00	.44	6.01	2.09	7.00	7.42	6.70	.61	4.46	.43	5.69	.60	4.37
12	10.9	.17	.23	1.16	4.00	.68	6.24	2.09	7.00	7.82	6.59	.60	4.39	.90	7.09	.60	4.37
13	5.5	.16	.34	1.23	2.08	.33	3.59	2.73	13.89	13.93	12.88	.67	14.30	---	3.63	.66	14.07
14	5.7	---	.20	1.17	2.33	.11	3.29	---	---	---	---	---	---	---	3.09	---	---
15	5.9	.09	.25	1.18	2.49	.22	3.78	3.16	8.89	8.88	8.55	.57	6.84	.28	3.62	.55	6.61
16	7.3	.11	.24	1.18	3.61	.39	5.50	3.16	8.89	9.25	8.54	.57	6.83	.47	5.05	.54	6.49
17	14.8	.19	.20	1.14	4.00	.77	6.14	6.35	18.00	19.60	16.75	.70	9.85	.91	6.74	.70	9.85
18	10.8	.19	.25	1.14	4.00	.77	6.32	6.35	18.00	20.93	17.04	.71	10.07	.91	6.55	.71	9.98
19	10.2	.19	.22	1.18	4.00	.77	6.37	6.35	18.00	19.46	16.80	.70	9.86	.91	6.94	.70	9.88
20	6.2	.19	.31	1.18	4.00	.77	6.73	6.35	18.00	21.21	17.25	.72	10.14	.91	6.60	.71	9.97
21	6.9	.23	.33	1.25	3.33	.77	6.04	6.35	18.00	19.22	16.74	.70	9.84	.91	5.77	.69	9.77
22	2.9	.23	.43	1.25	3.33	.77	6.35	6.35	17.55	21.78	17.15	.71	10.08	.91	5.47	.67	9.50
23	5.3	.09	.27	1.18	1.86	.16	2.84	11.80	28.46	27.92	27.43	.48	7.63	---	3.01	.47	7.47
24	5.5	.09	.26	1.18	2.11	.18	3.22	11.80	28.46	28.16	27.48	.48	7.63	---	3.39	.48	7.56
25	5.9	.09	.25	1.18	2.51	.23	3.83	11.80	28.46	28.44	27.46	.48	7.63	---	3.95	.47	7.45
26	6.3	.10	.25	1.18	2.83	.27	4.31	11.80	28.46	28.72	27.46	.48	7.63	---	4.41	.46	7.40
27	6.7	.10	.25	1.18	3.17	.32	4.84	11.80	28.46	29.01	27.45	.48	7.63	---	4.88	.46	7.39
28	7.2	.11	.24	1.18	3.53	.38	5.38	11.80	28.46	29.40	27.44	.48	7.62	---	5.36	.46	7.35
29	6.7	.15	.29	1.21	3.10	.48	5.13	11.80	55.29	55.79	51.31	.90	14.25	---	4.91	.90	14.26
30	7.9	.18	.27	1.21	3.96	.71	6.58	11.80	55.29	56.29	50.76	.89	14.09	---	6.21	.87	13.85
31	9.5	.25	.29	1.21	4.00	1.00	7.00	11.80	55.29	56.87	49.34	.86	13.70	---	7.26	.85	13.50
32	7.8	.58	.42	1.33	3.92	2.29	9.15	1.95	4.19	4.59	3.70	.42	5.29	2.48	8.93	.41	5.08
33	6.9	.52	.44	1.33	3.39	1.77	7.77	1.95	4.19	4.48	3.73	.43	5.34	1.72	7.66	.41	5.16

NACA

TABLE II.- SUMMARY OF AERODYNAMIC AND GEOMETRIC CHARACTERISTICS AND TEST CONDITIONS FOR RECTANGULAR WING-BODY COMBINATIONS

No.	Sketch	M_o	R	Wing Section	$\bar{c}$ (in.)	βA	$\frac{r}{s_m}$	$\frac{l_a}{r}$	$\frac{l_f}{r}$	Reference	Facility
1	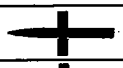	1.93	0.19×10^6	[1]b.c.	0.59	9.41	0.172	12.4	11.0	24	Langley 9 in.
2	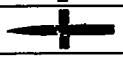	1.93	$.19\times10^6$	b.c.	.59	7.35	.210	12.4	11.0	24	Langley 9 in.
3	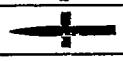	1.93	$.19\times10^6$	b.c.	.59	5.24	.273	12.4	11.0	24	Langley 9 in.
4		1.93	$.19\times10^6$	b.c.	.59	3.16	.382	12.4	11.0	24	Langley 9 in.
5		1.92	$.40\times10^6$	b.c.	1.25	5.64	.140	11.2	10.2	25	Langley 9 in.
6		1.28	$.56\times10^6$	[2]hex.	1.30	4.27	.153	8.8	13.1	19	Aberdeen
7	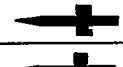	1.28	1.12×10^6	hex.	2.60	1.07	.265	7.6	12.2	19	Aberdeen
8		1.72	1.12×10^6	hex.	2.60	1.87	.265	7.6	12.2	20	Aberdeen
9		1.72	$.56\times10^6$	hex.	1.30	7.48	.153	8.8	13.1	20	Aberdeen
10		1.72	$.66\times10^6$	hex.	1.54	1.87	.379	0.0	21.5	20	Aberdeen
11		1.62	$.40\times10^6$	---	1.25	1.66	.350	6.8	9.8		Langley 9 in.
12		1.93	$.40\times10^6$	---	1.25	2.14	.350	6.8	9.8		Langley 9 in.
13		2.40	$.40\times10^6$	---	1.25	2.84	.350	6.8	9.8		Langley 9 in.
14		1.90	$.50\times10^6$	[3]d.w.	1.47	1.86	.384	0.0	14.5	27	Mich. U.
15		2.00	$.79\times10^6$	d.w.	3.00	4.76	.083	4.0	10.9		Ames 1x3 ft
16		1.50	$.91\times10^6$	d.w.	3.00	3.08	.083	4.0	10.9		Ames 1x3 ft
17		1.93	$.18\times10^6$	b.c.	.59	3.17	.382	12.4	11.0		Langley 9 in.
18		1.62	$.21\times10^6$	b.c.	.59	2.45	.382	12.4	11.0		Langley 9 in.
19		2.00	---	---	1.32	1.73	.333	0.0	24.0	26	Dainger-field
20		2.00	---	---	1.32	3.46	.200	0.0	24.0	26	Dainger-field

[1]b.c. indicates biconvex
[2]hex. indicates hexagonal
[3]d.w. indicates double wedge

TABLE II.- CONCLUDED

No.	$\beta A(1+\lambda)\left(\frac{1}{\beta A}+1\right)$	K_W	K_B	$K_W^{(s)}$	Theoretical									Experimental			
					Lift			Center of pressure						Lift		Center of pressure	
					$\beta(C_{L_\alpha})_W$	$\beta(C_{L_\alpha})_B$	$\beta(C_{L_\alpha})_c$	$\bar{l}_W$	$\bar{l}_{W(B)}$	$\bar{l}_{B(W)}$	$\bar{l}_c$	$(\bar{l}/l)_c$	$(\bar{l}/d)_c$	$\beta(C_{L_\alpha})_B$	$\beta(C_{L_\alpha})_c$	$(\bar{l}/l)_c$	$(\bar{l}/d)_c$
1	18.8	0.17	0.12	1.14	3.79	0.64	5.40	1.68	4.12	4.65	3.87	0.44	5.54	0.64	5.44	0.41	5.10
2	14.7	.22	.16	1.17	3.73	.82	5.76	1.68	4.12	4.65	3.83	.44	5.47	.82	5.47	.41	5.11
3	10.5	.32	.22	1.23	3.62	1.15	6.41	1.68	4.12	4.65	3.74	.43	5.35	1.15	6.69	.42	5.25
4	6.3	.56	.40	1.33	3.37	1.90	7.73	1.68	4.11	4.65	3.61	.41	5.15	1.90	7.16	.36	4.52
5	11.3	.06	.12	1.11	3.65	.23	4.71	1.68	4.12	4.78	4.11	.47	5.87	.23	4.37	.46	5.75
6	8.5	.06	.14	1.12	3.53	.22	4.67	3.18	8.82	9.37	8.61	.57	6.89	.19	5.08	.56	6.78
7	2.1	.10	.38	1.22	2.13	.22	3.63	3.18	8.56	9.54	8.45	.56	6.76	.19	3.46	.54	6.47
8	3.7	.13	.38	1.22	2.93	.38	5.07	3.18	8.78	9.88	8.60	.57	6.88	.40	4.70	.54	6.44
9	15.0	.10	.12	1.12	3.73	.38	5.00	3.18	8.83	9.69	8.48	.56	6.78	.40	5.36	.56	6.71
10	3.7	.37	.58	1.33	2.93	1.09	6.68	3.18	14.13	15.10	12.59	.84	10.07	1.14	6.38	.77	9.25
11	3.3	.27	.52	1.30	2.79	.76	5.84	1.77	4.82	5.49	4.59	.54	5.24	.80	4.71	.49	4.76
12	4.3	.32	.44	1.30	3.07	.98	6.32	1.77	4.85	5.63	4.54	.53	5.18	1.05	5.66	.50	4.90
13	5.7	.39	.38	1.30	3.30	1.29	6.84	1.77	4.87	5.82	4.46	.52	5.09	1.34	6.72	.51	4.92
14	3.7	.39	.59	1.33	2.92	1.13	6.74	2.06	8.30	9.23	7.49	.82	7.10	1.48	6.51	.75	6.51
15	9.5	- -	.08	1.06	3.58	.06	4.14	- -	- -	- -	- -	- -	- -	- -	4.11	- -	- -
16	6.2	- -	.09	1.06	3.35	.04	3.89	- -	- -	- -	- -	- -	- -	- -	4.05	- -	- -
17	6.3	.56	.40	1.33	3.37	1.90	7.73	1.68	4.11	4.65	3.61	.41	5.15	2.04	7.93	.37	4.60
18	4.9	.46	.45	1.33	3.18	1.47	7.13	1.68	4.10	4.55	3.69	.42	5.27	1.53	6.97	.37	4.68
19	3.5	.24	.50	1.28	2.84	.68	5.73	.76	8.48	9.17	7.74	.84	11.72	.68	5.48	.80	11.14
20	6.9	.10	.20	1.16	3.42	.34	4.98	.76	8.54	9.17	8.10	.88	12.27	.34	4.88	.84	11.69

TABLE III.- SUMMARY OF AERODYNAMIC AND GEOMETRIC CHARACTERISTICS AND TEST CONDITIONS FOR TRAPEZOIDAL WING-BODY COMBINATIONS

No.	Sketch	M_o	R	Wing Section	$\bar{c}$ (in.)	βA	λ	$\Lambda_{L.E.}$ (deg)	$\frac{\tau}{B_m}$	$\frac{l_a}{\tau}$	$\frac{l_f}{\tau}$	Reference	Facility
1		1.5	0.26×10^6	[1]d.w.	0.39	2.98	0.500	26.6	0.486	18.5	3.4	6	Ames 1x3 ft
2		2.0	$.26\times10^6$	d.w.	.39	4.62	.500	26.6	.486	18.5	3.4	6	Ames 1x3 ft
3	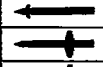	1.5	$.70\times10^6$	[2]hex.	1.06	3.30	.461	14.0	.250	5.9	14.5	6	Ames 1x3 ft
4		2.0	$.70\times10^6$	hex.	1.06	5.11	.461	14.0	.250	5.9	14.5	6	Ames 1x3 ft
5		1.5	$.56\times10^6$	hex.	.85	2.98	.500	20.5	.314	6.0	14.8	6	Ames 1x3 ft
6		2.0	$.56\times10^6$	hex.	.85	4.61	.500	20.5	.314	6.0	14.8	6	Ames 1x3 ft
7		2.0	$.46\times10^6$	d.w.	.77	4.62	.500	26.6	.486	18.5	3.4	8	Dainger-field
8		1.73	$.42\times10^6$	d.w.	.77	3.77	.500	26.6	.486	18.5	3.4	9	Dainger-field
9		2.25	$.52\times10^6$	d.w.	.77	5.38	.500	26.6	.486	18.5	3.4	9	Dainger-field
10		1.72	----	hex.	1.13	3.73	.500	20.5	.314	6.0	14.8	10	Aberdeen
11		1.73	$.92\times10^6$	hex.	1.70	3.77	.500	20.5	.314	6.0	14.8	9	Dainger-field
12		2.0	1.27×10^6	hex.	2.12	5.11	.461	14.0	.250	5.9	14.5	8	Dainger-field
13		2.0	1.02×10^6	hex.	1.70	4.61	.500	20.5	.314	6.0	14.8	7	Dainger-field
14		2.25	1.14×10^6	hex.	1.70	5.37	.500	20.5	.314	6.0	14.8	9	Dainger-field
15		1.96	2.03×10^6	d.w.	3.90	2.09	.302	60	.466	0	4.2		Langley 9 in.
16		1.28	1.05×10^6	hex.	2.49	1.07	.130	60	.265	9.9	6.7	12	Aberdeen
17		1.72	1.05×10^6	hex.	2.49	1.87	.130	60	.265	4.1	12.6	13	Aberdeen
18		1.28	$.80\times10^6$	hex.	1.90	1.60	.253	50	.228	11.2	7.4	12	Aberdeen
19		1.72	$.80\times10^6$	hex.	1.90	2.80	.253	50	.228	11.2	7.4	13	Aberdeen
20		1.93	$.27\times10^6$	hex.	.85	2.03	.305	60	.465	0	17.1	14	Langley 9 in.
21		2.40	$.47\times10^6$	hex.	1.79	2.11	.203	70	.356	0	16.6	15	Langley 9 in.
22		1.93	$.58\times10^6$	hex.	1.79	1.59	.203	70	.356	0	16.6	15	Langley 9 in.
23		1.72	$.80\times10^6$	hex.	1.90	2.80	.253	50	.228	4.4	14.2	13	Aberdeen
24		1.62	$.31\times10^6$	hex.	.85	1.57	.305	60	.465	0	19.0	16	Langley 9 in.
25		1.93	$.28\times10^6$	hex.	.85	2.03	.305	60	.465	0	19.0	16	Langley 9 in.
26		1.93	$.33\times10^6$	hex.	1.02	1.69	.323	15	.465	7.8	10.6	16	Langley 9 in.
27		1.93	$.24\times10^6$	hex.	.74	3.16	.352	45	.388	0	20.4	16	Langley 9 in.
28		1.93	$.83\times10^6$	hex.	2.57	1.03	.400	70	.356	0	14.5	16	Langley 9 in.
29		1.72	$.78\times10^6$	d.w.	1.86	3.75	.333	29.2	.228	.8	19.6	17	Aberdeen
30		1.28	$.46\times10^6$	d.w.	1.16	2.14	.333	29.2	.228	.8	19.6	18	Aberdeen
31		1.72	$.54\times10^6$	d.w.	1.28	3.76	.333	29.2	.300	16.6	5.0	17	Aberdeen
32		1.28	$.34\times10^6$	d.w.	.80	2.15	.333	29.2	.300	16.6	5.0	18	Aberdeen
33		1.28	1.24×10^6	hex.	2.89	1.07	.268	60	.265	7.3	10.1	19	Aberdeen
34		1.72	1.24×10^6	hex.	2.89	1.87	.268	60	.265	7.3	10.1	20	Aberdeen
35		1.28	1.17×10^6	hex.	2.73	1.07	.444	30	.265	6.8	11.4	19	Aberdeen
36		1.72	1.17×10^6	hex.	2.73	1.87	.444	30	.265	6.8	11.4	20	Aberdeen
37		2.87	$.60\times10^6$	d.w.	2.87	5.89	.387	22	.224	4.8	18.9	21	NAA 16x16 in.
38		2.87	$.79\times10^6$	d.w.	3.75	5.38	0	45	.232	3.8	17.9	21	NAA 16x16 in.
39		2.87	1.04×10^6	d.w.	4.94	3.11	0	60	.284	2.7	16.8	21	NAA 16x16 in.
40		1.93	$.30\times10^6$	hex.	.97	2.57	0	60	.382	10.8	10.1		Langley 9 in.
41		1.62	$.34\times10^6$	hex.	.97	1.99	0	60	.382	10.8	10.1		Langley 9 in.

[1]d.w. indicates double wedge.
[2]hex. indicates hexagonal.

TABLE III.- CONCLUDED

No.	$\beta A(1+\lambda)\left(\frac{1}{\beta^2}+1\right)$	K_W	K_B	$K_W^{(m)}$	Theoretical									Experimental			
					Lift			Center of pressure						Lift		Center of pressure	
					$\beta(C_{L_\alpha})_W$	$\beta(C_{L_\alpha})_W$	$\beta(C_{L_\alpha})_c$	$\bar{l}_W$	$\bar{l}_{W(B)}$	$\bar{l}_{B(W)}$	$\bar{l}_c$	$(\bar{l}/l)_c$	$(\bar{l}/d)_c$	$\beta(C_{L_\alpha})_B$	$\beta(C_{L_\alpha})_c$	$(\bar{l}/l)_c$	$(\bar{l}/d)_c$
1	6.5	1.38	0.56	1.44	3.49	4.83	11.81	1.03	2.01	2.44	1.72	0.15	1.72	4.31	11.05	0.13	1.50
2	8.9	2.00	.50	1.44	3.73	7.48	14.72	1.03	2.02	2.66	1.64	.14	1.64	7.97	16.29	.17	1.94
3	5.9	.16	.29	1.21	3.56	.57	5.91	1.03	7.89	8.51	7.34	.64	7.34	.59	6.10	.62	7.12
4	8.5	.24	.27	1.21	3.78	.89	6.48	1.03	7.92	8.78	7.11	.62	7.11	1.09	7.15	.61	7.04
5	6.0	.28	.41	1.27	3.50	.98	6.86	1.03	7.97	8.50	7.09	.62	7.09	1.01	7.15	.59	6.81
6	8.4	.41	.32	1.27	3.72	1.51	7.42	1.03	7.98	8.75	6.69	.58	6.69	1.86	8.20	.58	6.62
7	8.9	2.00	.50	1.44	3.73	7.48	14.72	2.06	4.01	5.39	3.28	.14	1.64	6.87	15.42	.17	1.93
8	7.7	1.67	.52	1.44	3.65	6.09	13.24	2.06	4.00	5.15	3.34	.14	1.67	5.68	12.21	.12	1.38
9	10.1	2.29	.48	1.44	3.80	8.70	16.00	2.06	4.01	5.62	3.22	.14	1.61	7.88	16.95	.14	1.60
10	7.1	.34	.34	1.27	3.62	1.22	7.05	1.27	10.65	11.50	9.17	.60	6.89	1.44	7.19	.58	6.66
11	7.2	.34	.33	1.27	3.62	1.23	7.02	2.06	15.97	17.26	13.71	.60	6.86	1.30	6.71	.60	6.83
12	8.5	.24	.26	1.21	3.78	.89	6.45	2.06	15.85	17.58	14.20	.62	7.10	.94	6.25	.60	6.93
13	8.4	.41	.32	1.27	3.72	1.51	7.42	2.06	15.97	17.53	13.38	.58	6.69	1.60	7.60	.57	6.50
14	9.6	.47	.31	1.27	3.77	1.76	7.72	2.06	15.99	17.75	13.08	.57	6.54	1.85	8.08	.56	6.42
15	5.5	.84	.61	1.41	2.95	2.48	8.44	2.06	9.38	12.02	7.98	.59	2.07	3.20	8.67	.65	2.29
16	3.8	.11	.39	1.22	2.04	.22	3.51	2.54	5.30	5.71	5.22	.43	5.22	.27	3.53	.41	4.93
17	4.7	.12	.33	1.22	3.06	.38	5.12	2.54	8.29	8.95	8.00	.67	8.00	.44	4.18	.63	7.52
18	5.0	.08	.26	1.19	2.64	.22	4.05	2.54	5.31	5.54	5.20	.43	5.20	.27	4.03	.43	5.12
19	6.5	.10	.23	1.19	3.68	.38	5.61	2.54	5.36	5.82	5.24	.44	5.24	.44	5.36	.41	4.89
20	5.4	.78	.57	1.41	3.12	2.42	8.60	1.50	7.85	8.41	6.17	.74	7.42	2.79	8.69	.62	6.20
21	5.7	.32	.40	1.31	3.13	1.01	6.37	1.09	8.51	9.15	7.46	.79	8.97	1.38	6.16	.72	8.23
22	5.1	.29	.43	1.31	2.58	.76	5.25	1.09	8.50	8.96	7.51	.79	9.04	.92	4.87	.77	8.76
23	6.5	.10	.23	1.19	3.68	.38	5.61	2.54	8.30	8.72	7.95	.66	7.95	.44	5.14	.64	7.71
24	4.8	.71	.67	1.41	2.62	1.87	7.32	1.50	8.62	9.05	6.90	.76	8.30	2.15	6.12	.68	7.43
25	5.4	.78	.57	1.41	3.12	2.42	8.60	1.50	8.63	9.19	6.73	.74	8.10	2.91	7.78	.64	6.99
26	4.6	.68	.63	1.41	2.94	2.01	8.01	1.50	4.89	5.82	4.25	.47	5.11	2.41	7.74	.41	4.46
27	6.9	.54	.37	1.34	3.67	1.99	8.27	1.09	9.10	9.65	7.25	.76	8.73	2.39	6.80	.66	7.49
28	3.8	.25	.54	1.31	1.94	.49	4.08	1.09	7.88	8.58	7.24	.76	8.71	.59	3.90	.73	8.29
29	7.1	.14	.25	1.19	3.73	.52	5.89	2.86	14.68	15.61	13.78	.84	10.14	.52	5.71	.84	9.60
30	4.9	.09	.28	1.19	3.27	.29	5.10	1.79	9.18	9.53	8.82	.86	10.38	.30	4.42	.87	10.50
31	7.1	.29	.33	1.25	3.73	1.08	6.98	2.86	4.35	5.24	4.27	.26	3.15	1.12	7.38	.22	2.70
32	4.9	.19	.37	1.25	3.27	.62	5.92	1.79	2.72	3.04	2.69	.26	3.16	.66	5.68	.22	2.71
33	4.3	.11	.33	1.22	1.97	.22	3.27	3.17	8.70	9.00	8.38	.56	6.71	.28	3.21	.55	6.55
34	5.3	.13	.30	1.22	2.94	.38	4.85	3.17	8.81	9.34	8.47	.56	6.78	.46	4.64	.54	6.51
35	2.6	.11	.39	1.22	2.06	.22	3.54	3.17	8.23	9.51	8.20	.55	6.57	.28	3.36	.53	6.35
36	3.8	.12	.39	1.22	3.08	.38	5.34	3.17	8.81	9.92	8.65	.58	6.93	.46	4.77	.54	6.45
37	9.4	.20	.24	1.18	3.85	.77	6.23	6.40	17.96	20.27	16.87	.70	9.93	.91	6.30	.71	9.97
38	7.4	.20	.33	1.19	3.85	.77	6.62	6.40	17.94	20.33	17.06	.71	10.04	.91	6.50	.69	9.78
39	5.1	.21	.42	1.24	3.65	.77	6.83	6.40	17.79	20.44	17.08	.71	10.06	.91	6.50	.69	9.78
40	5.3	.44	.52	1.33	3.53	1.54	8.06	1.50	4.31	4.86	3.90	.45	5.57	1.67	7.69	.43	5.39
41	4.7	.39	.54	1.33	3.05	1.19	6.89	1.50	4.30	4.74	3.92	.45	5.60	1.16	6.50	.43	5.42

NACA

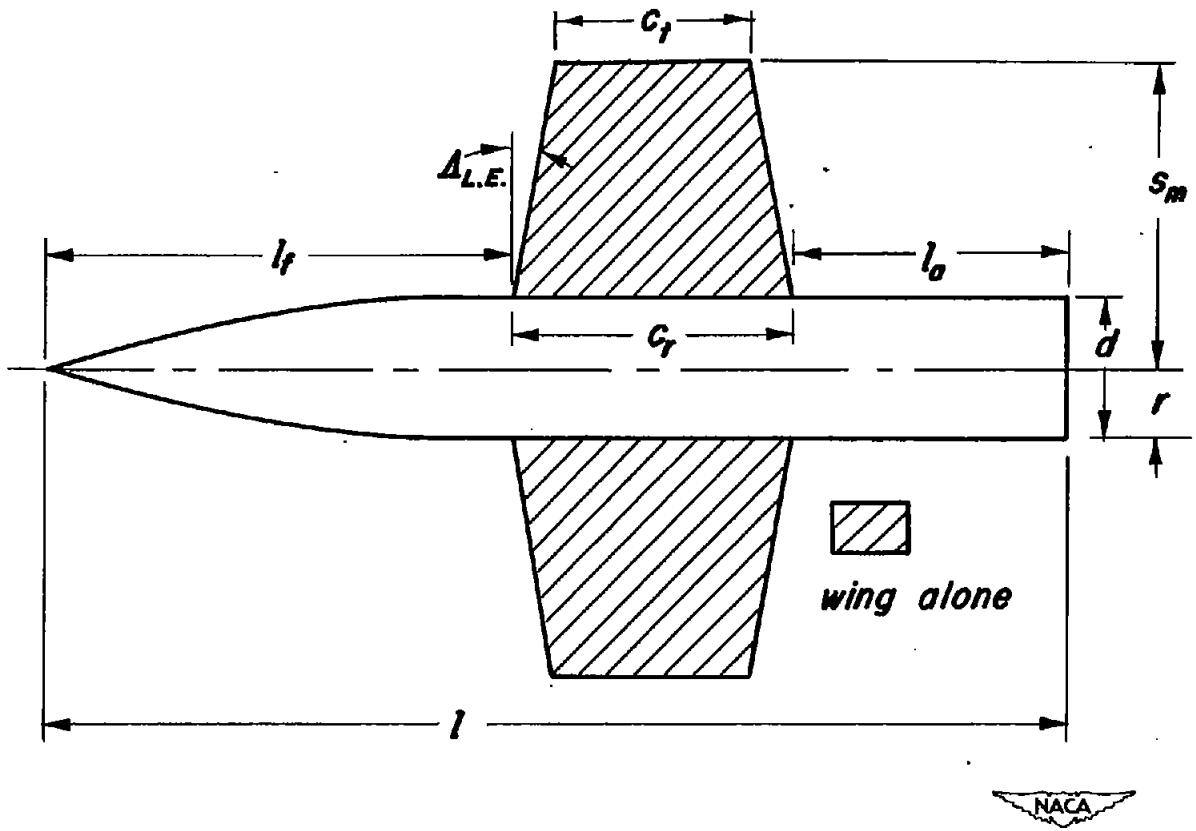

Figure 1.- Plan form dimensions for wing-body combinations.

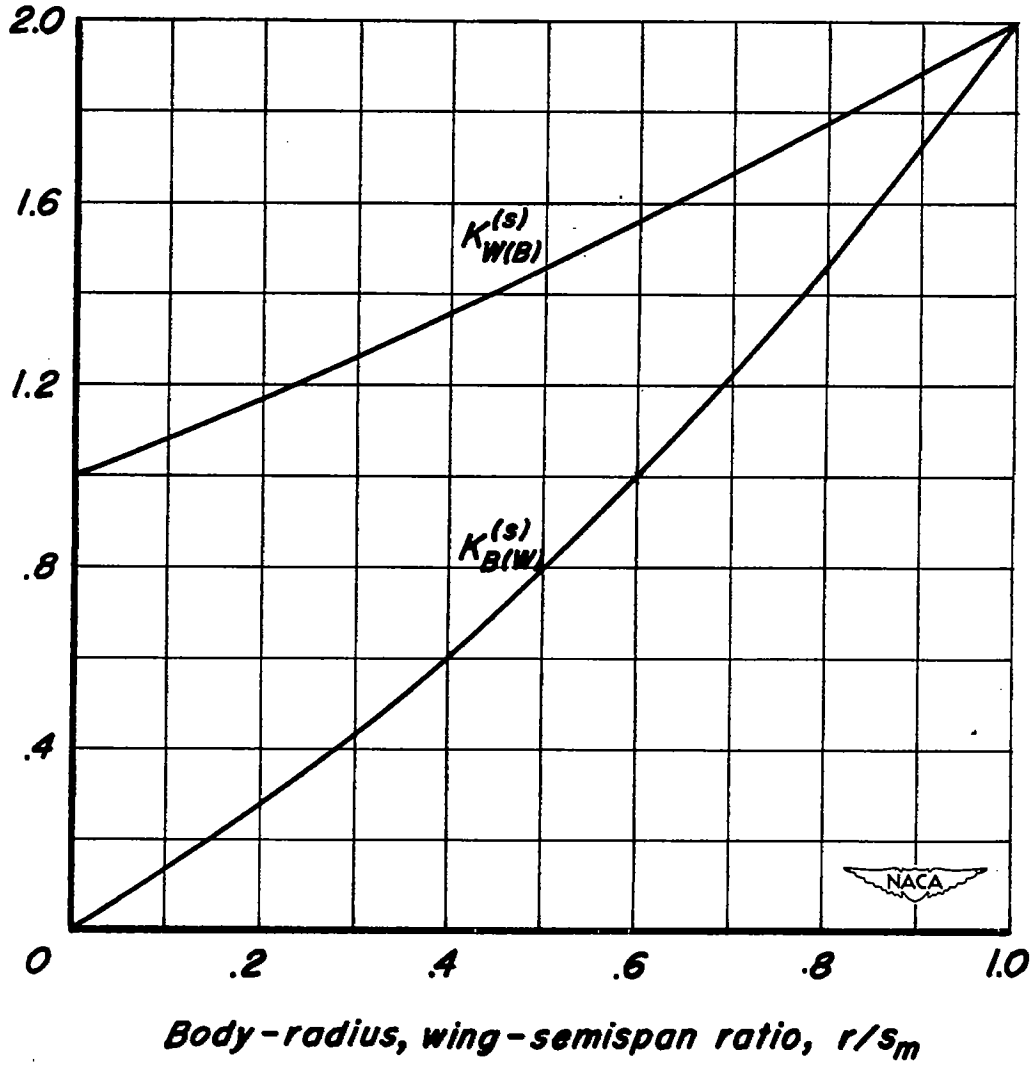

Figure 2.- Values of $K^{(s)}_{W(B)}$ and $K^{(s)}_{B(W)}$ from slender-body theory.

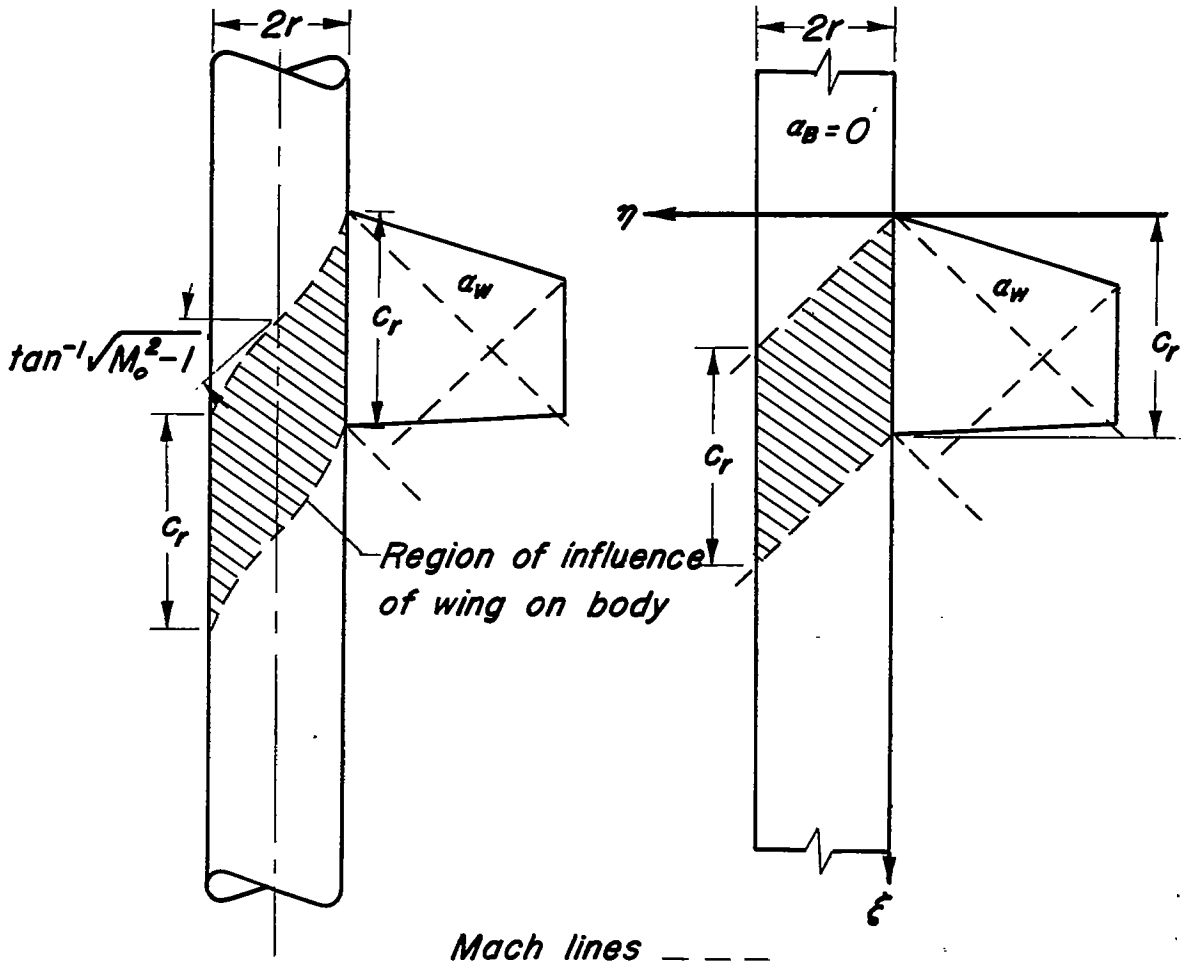

(a) Nonplanar case. (b) Equivalent planar case.

Figure 3. – Region of influence of half-wing on body.

[redacted]

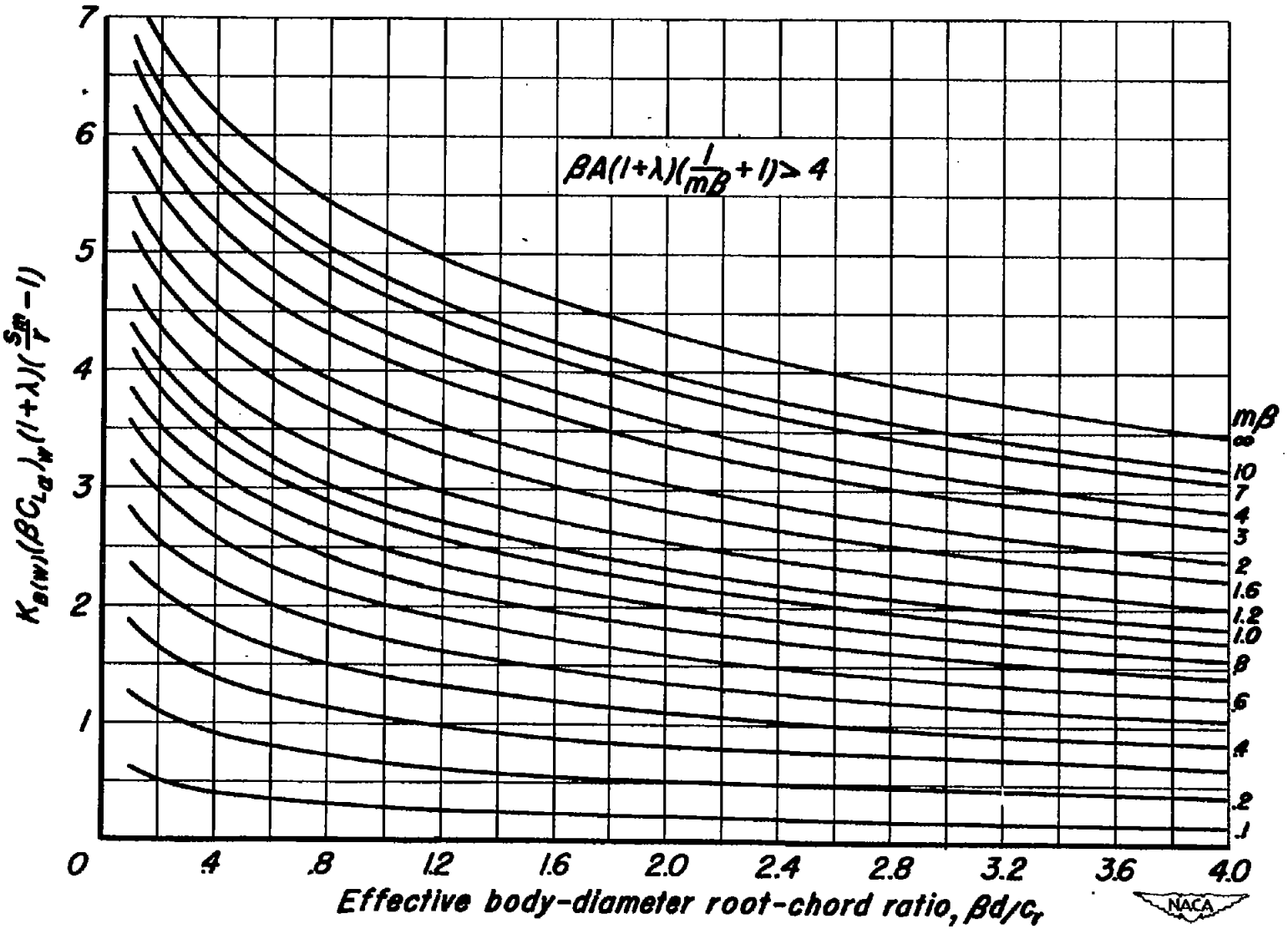

Figure 4.-Design chart for determining $K_{B(W)}$.

[redacted]

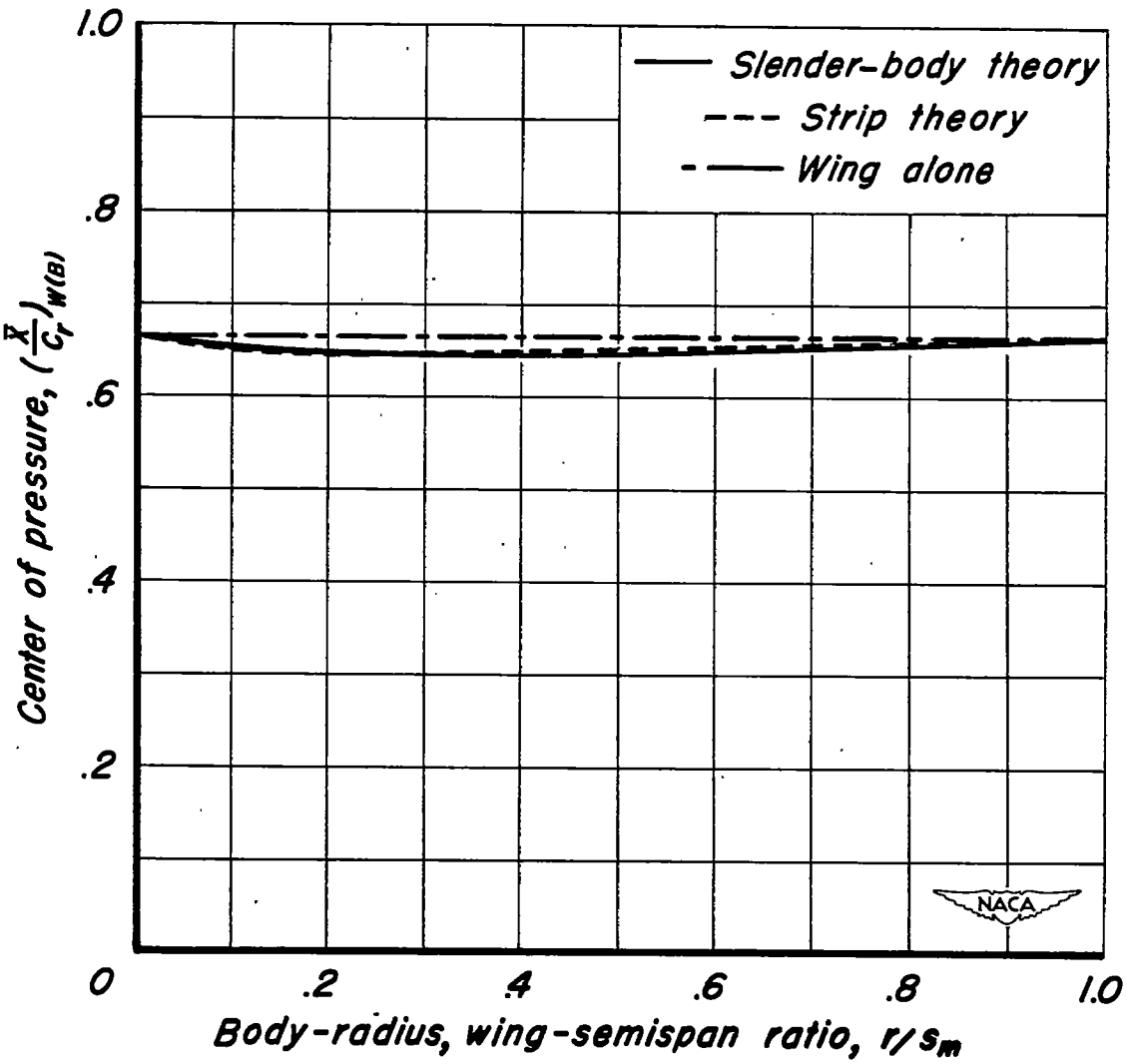

Figure 5.–Comparison of theoretical values of $(\frac{\bar{x}}{c_r})_{W(B)}$ for triangular wing with no trailing-edge sweep.

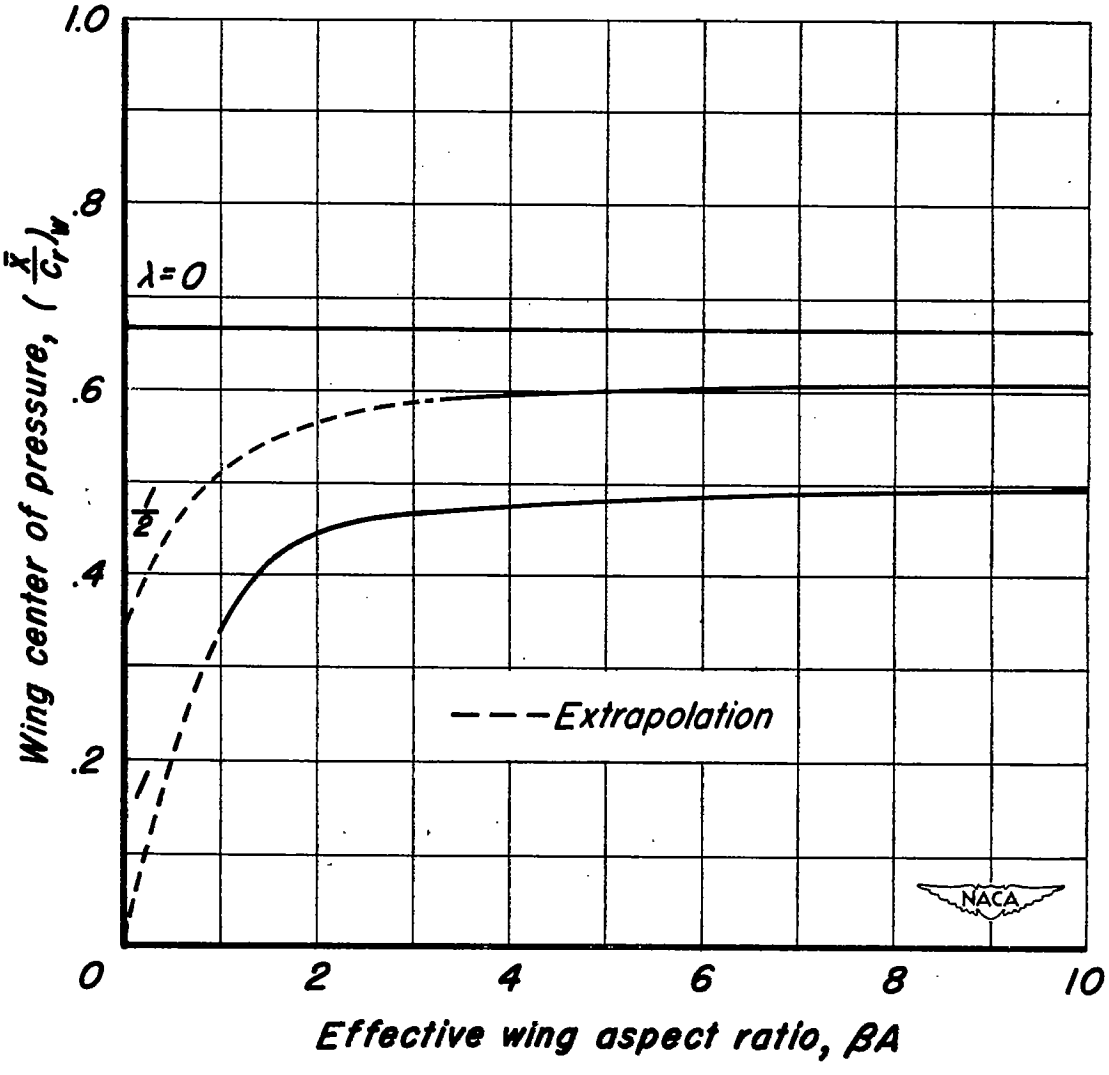

(a) No trailing-edge sweep.

Figure 6.- Center of pressure for wings according to linear theory.

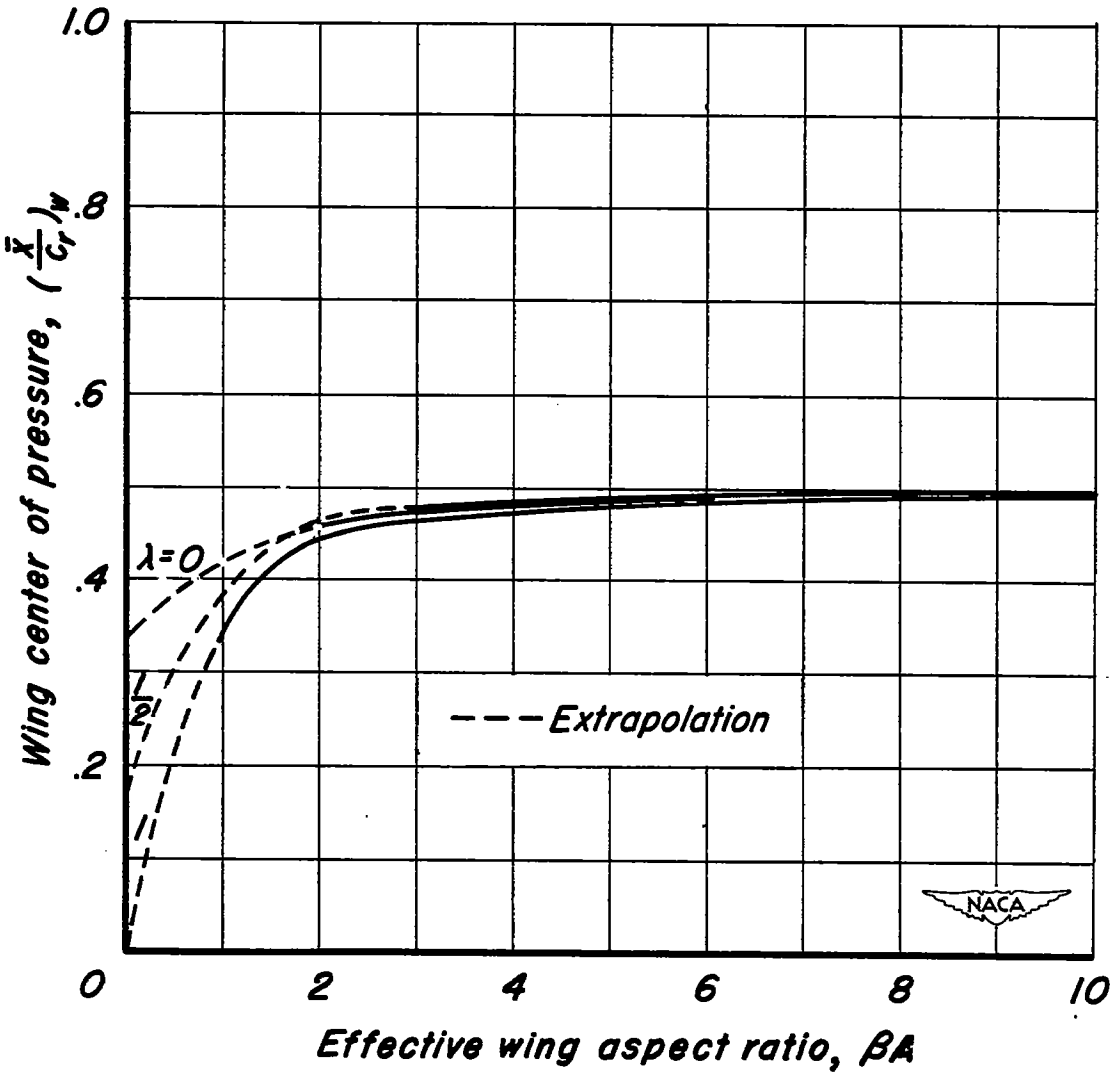

(b) No midchord sweep.

Figure 6.-Continued.

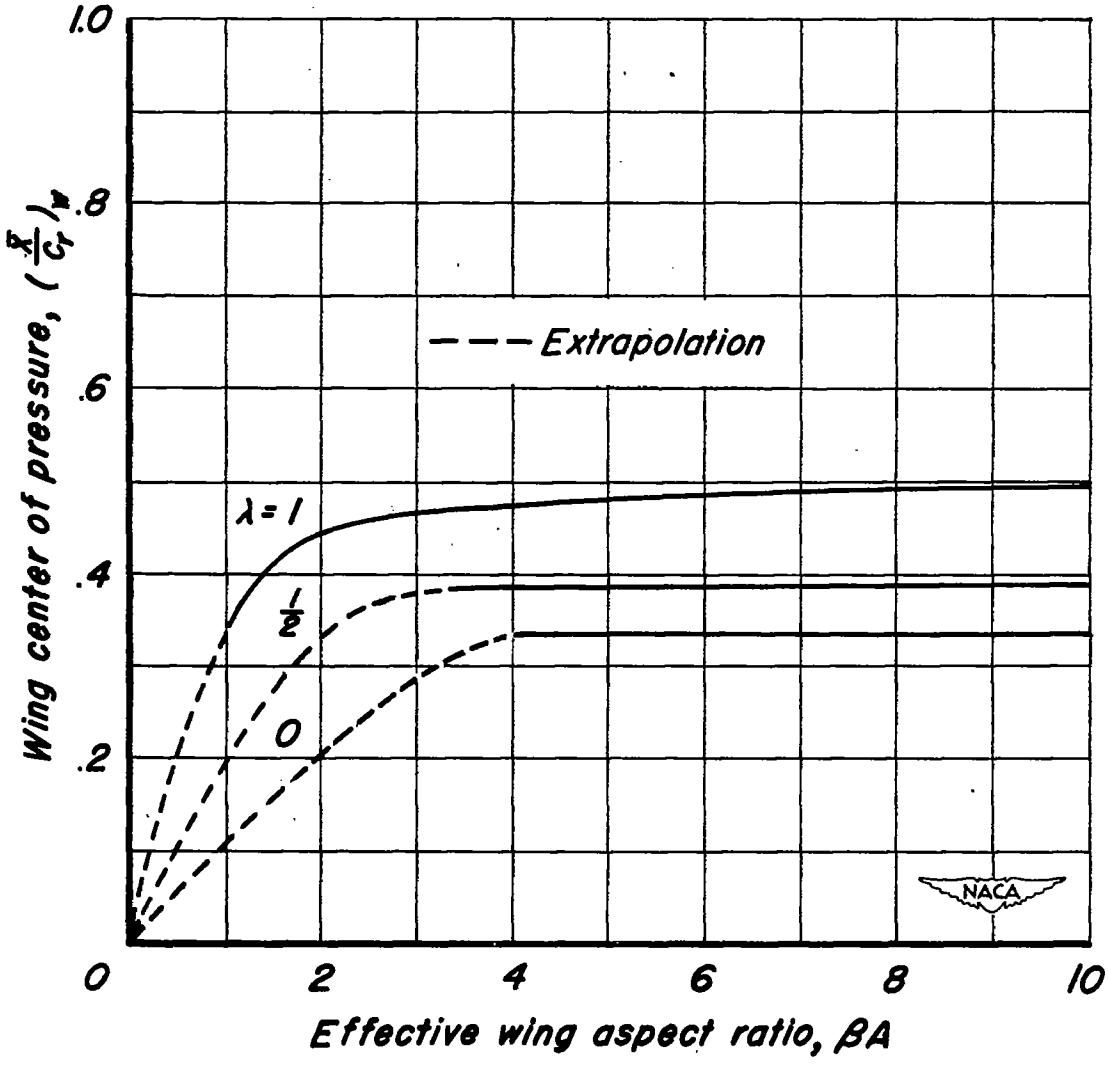

(c) No leading-edge sweep.

Figure 6.–Concluded.

[redacted]

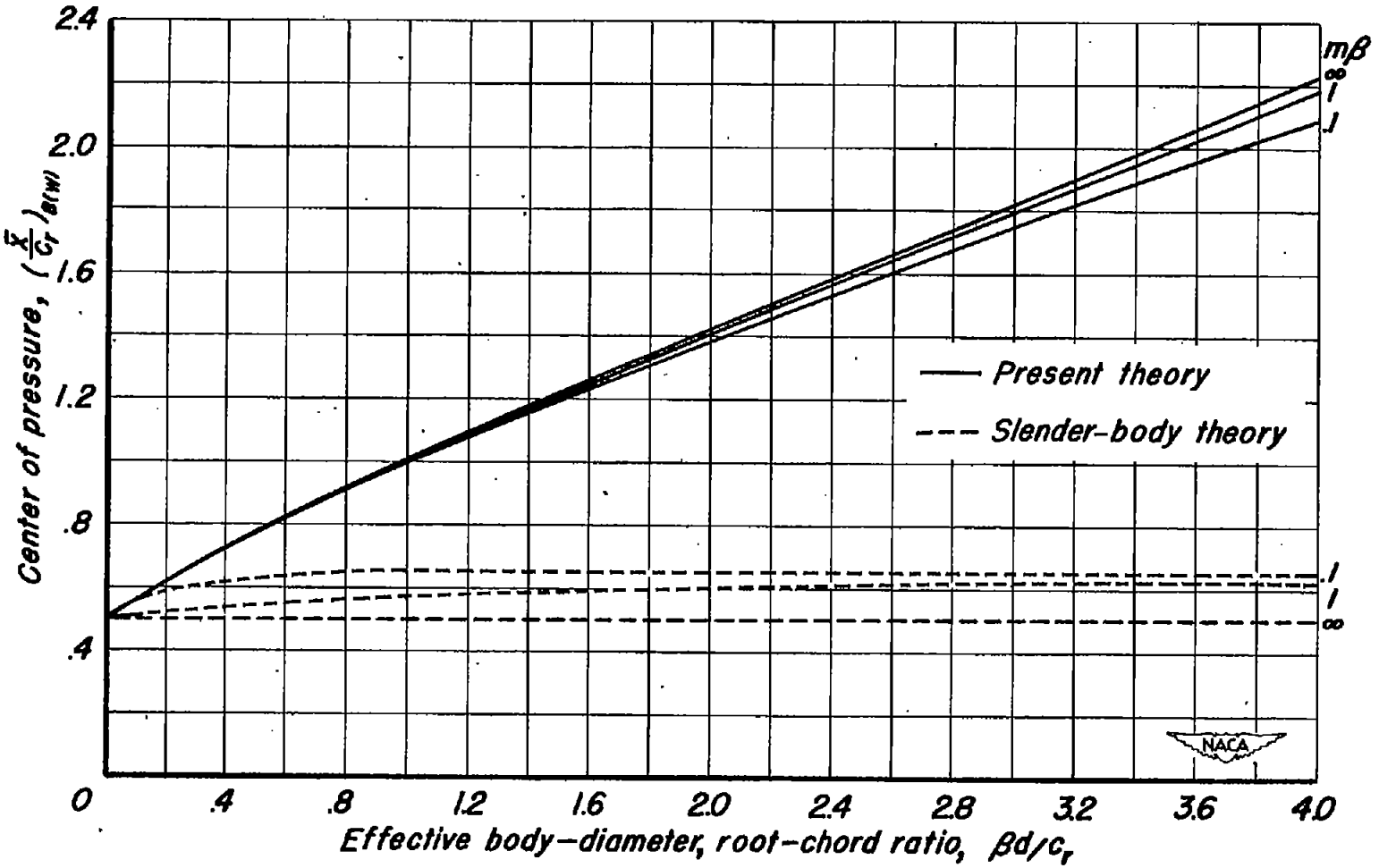

Figure 7.-Design chart for determination of $(\frac{\bar{X}}{c_r})_{B(W)}$.

[redacted]

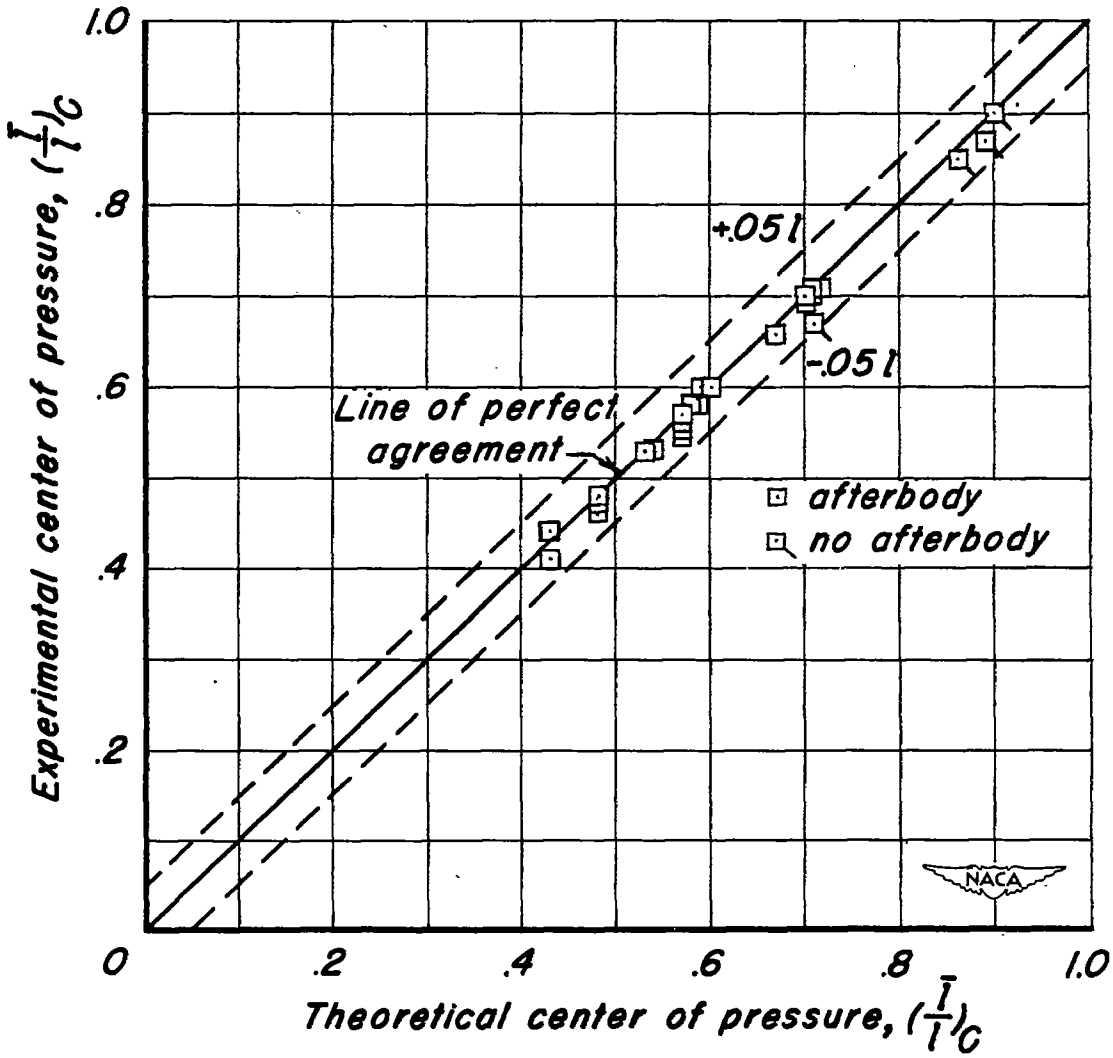

Figure 8.- Correlation between experimental and estimated centers of pressure for triangular wing-body combinations.

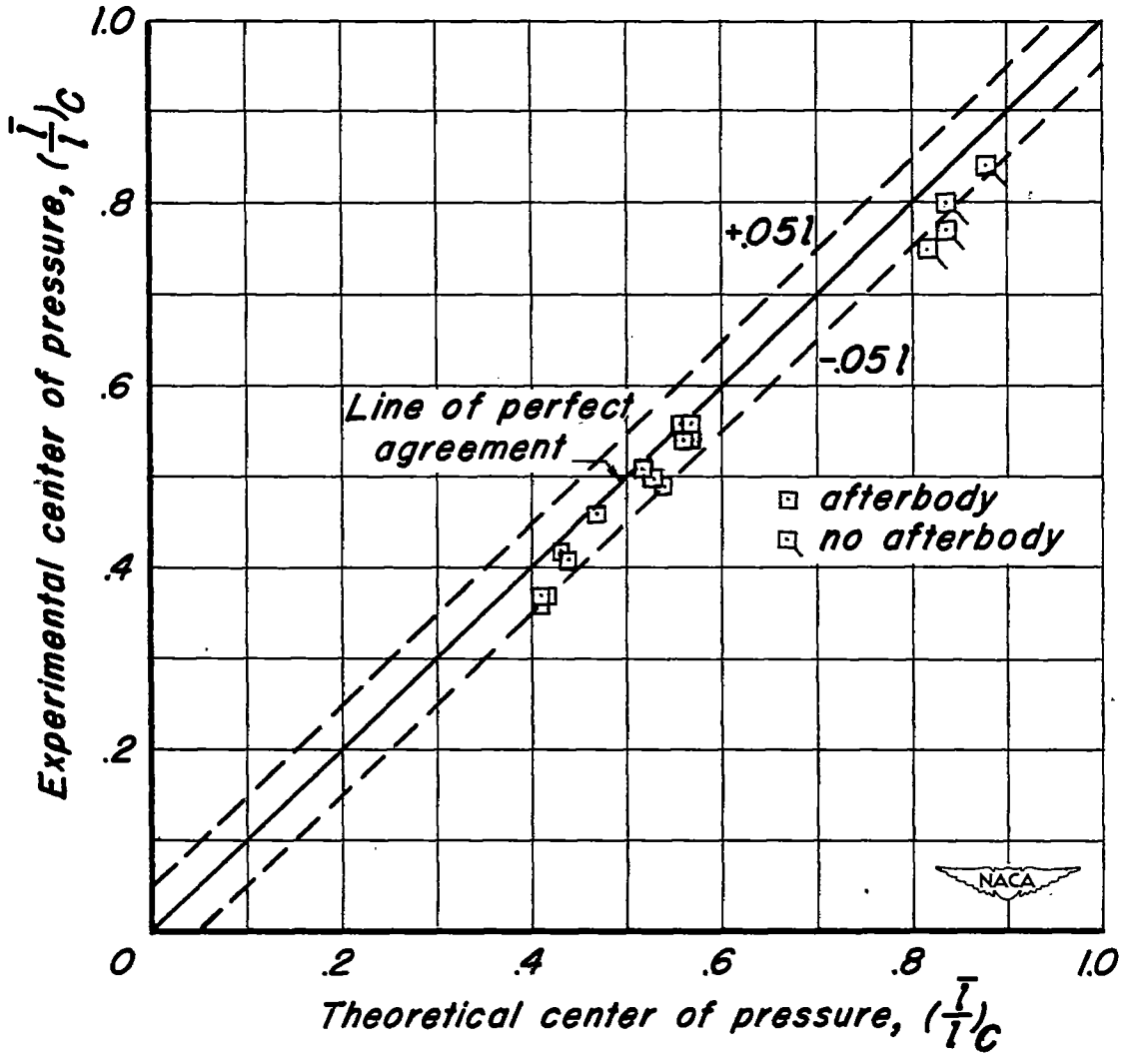

Figure 9.- Correlation between experimental and estimated centers of pressure for rectangular wing-body combinations.

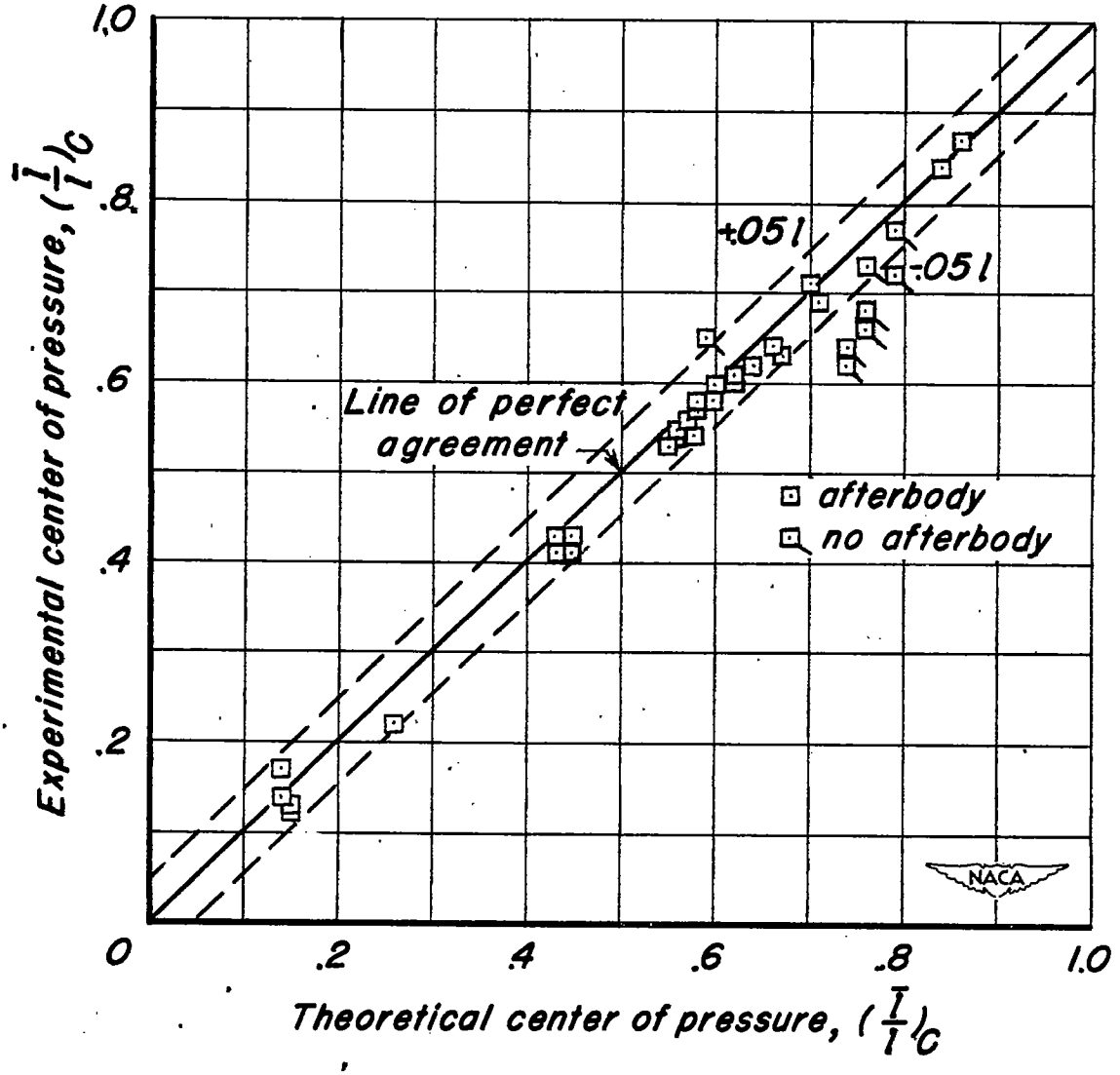

Figure 10.– Correlation between experimental and estimated centers of pressure for trapezoidal wing-body combinations.

[redacted]